Radiochim. Acta 99, 1–17 (2011) / DOI 10.1524/ract.2011.1853

Production and properties of transuranium elements

By Y. Nagame* and M. Hirata

Japan Atomic Energy Agency, Tokai, Ibaraki 319-1195, Japan

(Received February 28, 2011; accepted in revised form April 18, 2011)

Actinides / Syntheses / Electronic structure / Physical and chemical properties

Summary. We summarize historical perspective of the transuranium elements, neptunium (Np) through lawrencium (Lr), and recent progress on production, and nuclear and chemical properties of these elements. Exotic decay properties of heavy nuclei are also introduced. Chemical properties of transuranium elements in aqueous and solid states are summarized based on the actinide concept.

1. Introduction

Presently, we know more than 20 artificial elements beyond uranium as shown in Fig. 1. The history of the discovery of these elements is a fascinating story that has been described in the articles [1–3]. According to the actinide concept of Seaborg [4], the 5 *f* electron series ends with element 103, lawrencium (Lr), and a new 6*d* electron transition series is expected to begin with element 104, rutherfordium (Rf). The elements with $Z \geq 104$ are called transactinide elements. The currently known transactinide elements, elements 104 through 112, are placed in the periodic table under their respective lighter homologues in the 5*d* electron series, hafnium (Hf) to mercury (Hg). Elements from 113 to 118 synthesized would be in the successive 7*p* electron series, although the discoveries of elements with $Z \geq 113$ are still waiting to be confirmed. Searching for and producing new elements are very challenging subjects in advanced nuclear and radiochemistry. How many chemical elements may be synthesized on earth? How can they be produced?

How long can they survive? Which properties do determine their stability? What are their chemical and physical properties? And how are the orbital electron configurations affected in the strong electric field of heavy atoms? These are the most fundamental questions in science.

In the present review, we summarize the historical perspective of the transuranium elements, neptunium (Np) through lawrencium (Lr), and recent progress on production, and nuclear and chemical properties of these elements. Most part of this article is based on the modification of the previous review article [5]. The more comprehensive reviews on transuranium elements are published in [1, 2].

*Author for correspondence
(E-mail: nagame.yuichiro@jaea.go.jp).

2. Brief history of discovery of the transuranium elements

The discovery of transuranium elements with $Z = 93$ to 103 is summarized in Table 1. The names and symbols from element 101 through 103 were approved in 1992 by IUPAC (International Union of Pure and Applied Chemistry) based on the report of the Transfermium Working Group (TWG) [6] which consisted of scientists appointed by both IUPAP (International Union of Pure and Applied Physics) and IUPAC.

At the beginning, there were at least two difficulties in the discovery of transuranium elements; the first one was the chemical behavior of these elements. Before Seaborg's proposal of the actinide concept [4], it was believed that thorium (Th), protactinium (Pa), uranium (U), neptunium (Np), plutonium (Pu) and the next elements 95 and 96 should be placed as the heavier members of groups 4 through 10. Based on the actinide concept, however, it was expected that the new series should start with actinium (Ac) as a prototype and end with the filling of the 5 *f* electron shell at element 103, and that the heavier actinides would be trivalent homologues of the lanthanide series in which 4 *f* orbitals were being filled. The second difficulty was the method of identification of transuranium nuclides produced in nuclear reactions. A nuclide to be identified had to be isolated before it decayed from large quantities of impurities, especially from fission products.

In the following, the discovery of each transuranium element is briefly summarized.

2.1 Neptunium (Np)

The first man-made transuranium element, neptunium (Np), was discovered by McMillan and Abelson [7] while studying the neutron-induced fission of uranium (U). The reaction used in the synthesis was

TS

$$^{238}\mathrm{U}(n,\gamma)^{239}\mathrm{U} \xrightarrow[23\ \mathrm{min}]{\beta^-} {}^{239}\mathrm{Np} \xrightarrow[2.3\ \mathrm{d}]{\beta^-} \quad (1)$$

For separating fission products from the neutron capture ones, a recoil technique was employed; fission products recoiling out of the target foil with high kinetic energies were removed from the target, and the non-recoiling neutron capture products together with the target material were subjected to chemical separations. It was found that in the presence of the reducing agent, sulfur dioxide SO_2, the 2.3-d

TS Please check all equations.

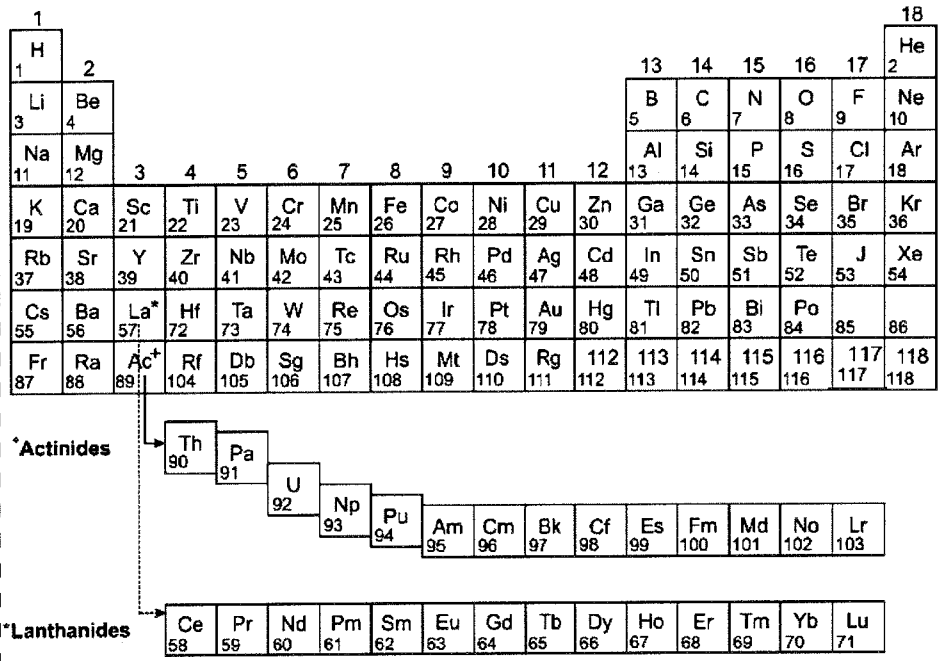

Fig. 1. Periodic Table of the Elements. The arrangement of the early actinides reflects that these elements resemble, to a decreasing extent, those in groups 4–8. The transactinide elements 104 through 112 form the 6*d* transition element series and take the positions below Hf through Hg. Elements 113 to 118 are the 7*p* elements.

Atomic number	Element	Symbol	Year of discovery	Production reaction
93	Neptunium	Np	1940	$^{238}U(n,\gamma)^{239}U \rightarrow {}^{239}Np(2.3\,d)$
94	Plutonium	Pu	1940–1941	$^{238}U(d,2n)^{238}Np \rightarrow {}^{238}Pu(87.7\,y)$
95	Americium	Am	1944–1945	$^{238}U(\alpha,n)^{241}Pu \rightarrow {}^{241}Am(433\,y)$
96	Curium	Cm	1944	$^{239}Pu(\alpha,n)^{242}Cm(163\,d)$
97	Berkelium	Bk	1949	$^{241}Am(\alpha,2n)^{243}Bk(4.5\,h)$
98	Californium	Cf	1950	$^{242}Cm(\alpha,n)^{245}Cf(44\,min)$
99	Einsteinium	Es	1952	Thermonuclear explosion, ^{253}Es (20 d)
100	Fermium	Fm	1952	Thermonuclear explosion, ^{255}Fm (22 h)
101	Mendelevium	Md	1955	$^{253}Es(\alpha,n)^{256}Md(1.3\,h)$
102	Nobelium	No	1958	$^{244}Cm(^{12}C,4n)^{252}No(\sim 3\,s)$
103	Lawrencium	Lr	1961	$^{249-252}Cf(^{10,11}B,xn)^{258}Lr(\sim 4\,s)$

Table 1. Discovery of transuranium elements with atomic numbers 93 through 103.

half-life species produced in the growth from the 23-min U was quantitatively precipitated as a fluoride complex. This behavior chemically distinguished the products from U.

The later chemical study showed that Np was oxidized to the pentavalent state with the oxidizing agent, bromate ion BrO_3^-; it resembled uranium, not rhenium (Re), contrary to the expectation from the periodic table at that time. The result was the first evidence that an inner electron shell, the 5 *f* shell, is filled in the transuranium elements. The isotope of Np with the longest half-life ($T_{1/2} = 2.14 \times 10^6$ y) is ^{237}Np, the mother nuclide of the neptunium decay series produced in nuclear reactors. Neptunium was named after the planet Neptune, the next planet beyond Uranus.

2.2 Plutonium (Pu)

Plutonium (Pu), the second transuranium element, was discovered by Seaborg *et al.* [8]. The first isotope of Pu was synthesized by using the 60 inch cyclotron at the University of California, Berkeley in the deuteron bombardment of U,

$$^{238}U(d,2n)^{238}Np \xrightarrow[2.1\,d]{\beta^-} {}^{238}Pu \xrightarrow[87.7\,y]{\beta^-} \quad (2)$$

The α-emitting product was identified as a new element from the study of chemical behavior of this isotope. It was distinctly different from both U and Np in its redox properties; the 3+ and 4+ valence states were more stable. A second isotope of element 94, ^{239}Pu, with $T_{1/2} = 24\,000$ y was synthesized very shortly thereafter as a daughter of the β^- decay of ^{239}Np, which confirmed the presence of element 94. The isotope ^{239}Pu produced in appreciable amounts in nuclear reactors is of major importance, because of its large fission cross section with thermal neutrons. It was named after the planet Pluto in analogy to U and Np.

2.3 Americium (Am) and curium (Cm)

Element 95, americium (Am), and element 96, curium (Cm) were synthesized by Seaborg *et al.* and Ghiorso *et al.* as follows [1, 9].

$$^{239}Pu(n,\gamma)^{240}Pu(n,\gamma)^{241}Pu \xrightarrow{\beta^-} {}^{241}Am \xrightarrow[433\,y]{\alpha},$$
$$^{239}Pu(\alpha,n)^{242}Cm \xrightarrow[163\,d]{\alpha} {}^{238}Pu\,, \quad (3)$$

The isotope ^{242}Cm was identified by observing the known isotope ^{238}Pu as the α-decay daughter of the new isotope,

while ^{241}Am was produced through the successive neutron capture reactions in ^{239}Pu.

The elements Am and Cm are quite similar to the rare earth elements in their chemical properties; a stable oxidation state is 3+. It was too difficult for the discovery team to chemically isolate the two elements from each other and from rare earth fission products. For their chemical separation, the development of an ion-exchange technique was required which also made feasible the separation and identification of subsequent transuranium elements. Element 95, americium, was named after the Americas in analogy with the naming of its rare earth homologue, europium (Eu), and curium was named after Marie and Pierre Curie in analogy with the naming of its homologue, gadolinium (Gd), that was named after the Finnish rare earth chemist Johann Gadolin.

2.4 Berkelium (Bk) and californium (Cf)

The element with the atomic number 97, berkelium (Bk), was produced in irradiation of milligram amounts of ^{241}Am with α particles at Berkeley [10]:

$$^{241}\mathrm{Am}(\alpha, 2n)^{243}\mathrm{Bk} \xrightarrow[4.5\ \mathrm{h}]{\mathrm{EC},\alpha} \quad (4)$$

To identify the new isotope, a rapid cation-exchange separation technique using ammonium citrate as an eluant was employed. Early experiments indicated that element 97 had two oxidation states 3+ and 4+. The actinide concept provided the guidance to search for these two oxidation states, by analogy with the homologue element, terbium (Tb). The chemically separated samples were subjected to the measurement of radiation. Characteristic Cm X-rays associated with the electron capture (EC) decay and low intensity α particles with $T_{1/2} = 4.5$ h were detected. Berkelium was named after the city of Berkeley, California where it was discovered, just as the name terbium derived from Ytterby, Sweden.

Californium (Cf) was synthesized in 1950 by irradiation of a few micrograms of ^{242}Cm with α particles:

$$^{242}\mathrm{Cm}(\alpha, n)^{245}\mathrm{Cf} \xrightarrow[44\ \mathrm{min}]{\alpha,\mathrm{EC}} \quad (5)$$

The identification of element 98 was accomplished with a total of only 5000 atoms [11]. The ion-exchange techniques were also used in the separation and identification of Cf. Element 98 was eluted in the expected fraction, and the observed half-life and α-particle energy of the radioactivity were also in agreement with predictions. It was named after the state of its discovery.

The last four actinides (Am, Cm, Bk and Cf) have 3+ as their most stable valence state in solution, just as the rare earth elements. The similarity in solution has been commonly used for identification of a particular actinide.

2.5 Einsteinium (Es) and fermium (Fm)

Einsteinium (Es) and fermium (Fm) were identified in 1952 in the radioactive debris from the 'Mike' thermonuclear explosion that took place in the Pacific. Ion-exchange separation was applied, and the new elements, Es and Fm, were isolated by processing larger amounts of the radioactive coral material [12]. Chemical identification was made by ion-exchange separations, while isotopic assignments were made as the result of the corresponding decay sequences: $^{253}\mathrm{Cf} \rightarrow {}^{253}99$ and $^{255}99 \rightarrow {}^{255}100$. A 20-d radioactivity emitting α particles of 6.6 MeV was identified as ^{253}Es and a 7.1-MeV α activity with $T_{1/2} = 22$ h was identified as ^{255}Fm. The elements Es and Fm were named in honor of Albert Einstein and Enrico Fermi, respectively. These discoveries confirmed that ^{238}U can suffer as many as 17 successive neutron captures and subsequent β^- decays.

2.6 Mendelevium (Md)

Mendelevium (Md) was produced in 1955 by irradiation of ^{253}Es with α particles [13]. The number of atoms of element 101, N_{101}, expected to be produced was calculated as: $N_{101} = N_{\mathrm{Es}}\phi_\alpha\sigma t \approx 1$ atom under the experimental conditions characterized by the following parameters. The number of the ^{253}Es target atoms was $N_{\mathrm{Es}} \approx 10^9$ ($\sim 4 \times 10^{-13}$ g), the flux density of α particles was $\phi_\alpha \approx 10^{14}$ particles s^{-1}, the cross section was $\sigma \approx 1$ mb ($= 10^{-27}$ cm^2), and the irradiation time was $t \approx 10^4$ s. The Es target was prepared by electrodeposition on a thin gold foil. To detect these single atoms produced in 10^4 s, the recoil technique was applied. The produced element 101, recoiling through a vacuum due to the momentum of the impinging α particles, could be caught on a catcher foil. After irradiation, the catcher foil containing recoiling Md atoms was subjected to chemical separation by the cation-exchange resin Dowex-50 with an eluant of ammonium α-hydroxy isobutyrate (α-HIB). Spontaneous fission (SF) events with a half-life of 3.5 h were observed in the fractions corresponding to elements 100 and 101. At that time, it was assumed that the isotope $^{256}101$ was produced in the $^{253}\mathrm{Es}(\alpha, n)$ reaction that decayed by EC with a half-life of the order of half an hour to ^{256}Fm, and that ^{256}Fm then decayed by spontaneous fission (SF) with a half-life of about 3.2 h. In fact, another experiment confirmed the SF decay of ^{256}Fm.

Only 17 atoms of Md were detected by their EC decay into the spontaneously fissioning nuclide ^{256}Fm that is presently known to have the half-life of 2.6 h:

$$^{253}\mathrm{Es}(\alpha, n)^{256}\mathrm{Md} \xrightarrow[1.3\ \mathrm{h}]{\mathrm{EC}} {}^{256}\mathrm{Fm} \xrightarrow[2.6\ \mathrm{h}]{\mathrm{SF}} \quad (6)$$

The name mendelevium was suggested for the element, in honor of the Russian chemist, Dmitri Mendeleev.

2.7 Nobelium (No) and lawrencium (Lr)

The first report of the discovery of element 102 came from the Nobel Institute, Stockholm, Sweden. The research group used the reaction of $^{244}\mathrm{Cm} + {}^{13}\mathrm{C}$ in which they found a new α emitter with a half-life of about 10 min. Experiments neither at Berkeley nor at the Kurchatov Institute in Moscow, however, confirmed the above result. In 1958 Ghiorso *et al.* [14] announced the positive identification of ^{254}No that was supposedly produced in the following reaction by use of the double recoil technique:

$$^{246}\mathrm{Cm}(^{12}\mathrm{C}, 4n)^{254}\mathrm{No} \xrightarrow[T_{1/2}\approx 3\ \mathrm{s}]{\alpha} {}^{250}\mathrm{Fm} \xrightarrow[30\ \mathrm{min}]{\alpha} \quad (7)$$

The nuclide ^{250}Fm, the daughter of the new element, was collected using the recoil technique, one atom at a time, and identified as Fm by their position in the cation-exchange elution curve. A half-life of ~ 3 s was assigned to ^{254}No at that time. It is now known that, however, the 3-s radioactivity was ^{252}No produced in the ^{244}Cm(^{12}C, 4n) reaction; the used target contained 20 times more ^{244}Cm than ^{246}Cm. ^{254}No is now known to have a 55-s half-life. The errors in this experiment indicate the difficulty associated with one-atom-at-a-time studies. In subsequent chemical experiments, it was found that the most stable oxidation state of element 102 in solution was 2+ [15]. The element was named nobelium after Alfred Nobel.

The first identification of an isotope of element 103 was conducted by the Berkeley group in 1961 [16]. The californium isotopes, ^{249,250,251,252}Cf, were bombarded with boron beams:

$$^{249,250,251,252}\mathrm{Cf}(^{10,11}\mathrm{B}, xn)^{258}\mathrm{Lr} \xrightarrow[4.3\ \mathrm{s}]{\alpha} \qquad (8)$$

Reaction products recoiling from the target were caught by a long metallized Mylar tape which was moved to a series of α-particle detectors. A new α-emitting nuclide with α energy of 8.6 MeV and a half-life of ~ 4 s was assigned to ^{257}Lr. Later experiments, however, indicated this radioactivity was due to ^{258}Lr. Subsequent identification of element 103 was made by the Russian group in 1965 using the double recoil technique [17].

Lr is the first actinide that was identified through a purely instrumental method, because the half-life of the isotope was too short to allow any chemistry. Silva *et al.* later conducted, however, the ion-exchange experiments of ^{256}Lr ($T_{1/2} = \sim 30$ s) and confirmed that Lr exhibits a stable 3+ state in solution [18], as expected by the actinide concept. Lawrencium was named after Ernest O. Lawrence, the inventor of the cyclotron.

3. Production of transuranium nuclides

There are two kinds of methods for production of transuranium elements as indicated in the previous section: neutron capture reactions in nuclear reactors and charged-particle-induced reactions at accelerators.

3.1 Neutron capture reactions

The method is based on the concept that absorption of neutrons by nuclides with the atomic number Z leads to formation of neutron-rich nuclides that transmutate by β^- decay into nuclides with the atomic number $Z+1$.

Four of the transuranium elements (Np, Am, Es, and Fm) were first produced using neutron capture reactions. In Fig. 2, the neutron capture paths used for production of transuranium nuclides in nuclear reactors are shown. Starting with ^{238}U, the main path goes to ^{239}Pu that undergoes multiple neutron captures to ^{243}Pu. The nuclide ^{243}Pu decays to ^{243}Am that successively undergoes captures and decays to ^{244}Cm. Then ^{244}Cm can undergo multiple neutron captures to yield the Cm isotopes up to ^{249}Cm followed by subsequent

Fig. 2. Neutron capture paths to produce transuranium nuclides in nuclear reactors. The horizontal arrows represent the neutron capture and the vertical ones pointing upwards indicate β^- decay. The main paths are shown by the solid arrows.

captures and decays to ^{249}Bk, ^{250}Bk, ^{250}Cf, ^{252}Cf and finally to ^{257}Fm. The chain ends at the 380-μs SF of ^{258}Fm.

3.2 Charged-particle-induced reactions

Compound nucleus reactions involving light incident charged particles were used for the first production of the transuranium elements Pu, Cm, Bk, Cf, and Md. For the production of transuranium nuclei far from the stability-line, however, the emphasis has shifted from using light charged-particle-induced reactions to using heavy-ion-induced reactions. Recent developments in accelerator technology have made possible the use of high intensity heavy-ion beams as massive as ^{238}U.

Successful production of fissioning nuclei, such as transuranium nuclides in nuclear reactions, depends mainly on two factors: fusion cross section, σ_{fusion}, and survival probability, P_{survival},

$$\sigma_{\text{production}} = \sigma_{\text{fusion}} \times P_{\text{survival}} . \qquad (9)$$

The first term is the yield of compound nucleus formation or the fusion cross section used in the heavy-ion reaction, while the second term is the survival probability of the produced transuranium nucleus in the process of de-excitation. Fusion cross section can be approximated by the equation

$$\sigma_{\text{fusion}} = \pi \bar{\lambda}^{-2} \sum_{l=0}^{l_{\text{fusion}}} (2l+1)\, T_l P_{\text{CN}} \qquad (10)$$

where $\bar{\lambda}$ is the de Broglie wave length of the incident particle, l is the orbital angular momentum and T_l indicates the transmission coefficient of the wave. P_{CN} is the probability of the compound nucleus formation. In the de-excitation process of transuranium nuclei, competition between the particle emission (mainly neutron) and fission that destroys transuranium nuclei, Γ_n/Γ_f, should be taken into account, where Γ_n and Γ_f denote decay widths for neutron emission and fission, respectively. The survival probability P_{survival} depends mainly on Γ_n/Γ_f as,

$$P_{\text{survival}} \approx \prod_{i=1}^{x} \left(\frac{\Gamma_n}{\Gamma_f}\right)_i \approx \prod_{i=1}^{x} \exp\left[(B_f - B_n)/T\right]_i \qquad (11)$$

where B_f and B_n are fission barrier and neutron separation energy of the compound nucleus, respectively, T is the nuclear temperature, and x is the number of emitted neutrons. The systematically decreasing trend of the production cross section of heavy nuclei with increasing Z is given in [3, 19] and also in the contributions by Hofmann and Oganessian of this issue.

In the production of heavy nuclei with heavy ions, additional factors that enhance or decrease the yields of transuranium products should be considered. They are fusion enhancement at sub-barrier energy and dynamical hindrance to fusion. The dynamical hindrance caused by the Coulomb repulsion between two fusing nuclei in heavy nuclear systems brings up a serious problem for heavy element production. Experimental data and recent interpretation of the dynamical fusion hindrance are summarized in the review article by Armbruster [20]. The anomalous sub-barrier fusion of two

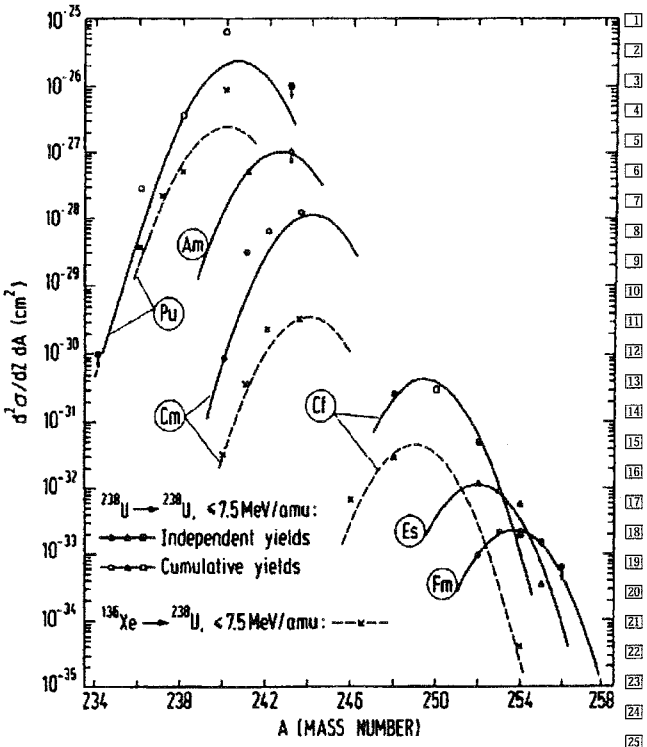

Fig. 3. Production cross sections of transuranium nuclides in the reactions $^{238}U + ^{238}U$ and $^{238}U + ^{136}Xe$ [22].

massive nuclei is the phenomenon that is several orders of magnitude larger than expected from the quantum tunneling through the interaction barrier. Various theoretical attempts have been made to understand the causes of this enhancement of fusion, such as static deformation of colliding nuclei, neck formation during fusion, vibrational excitation of nuclear surfaces, and nuclear structure effects. The detailed description of the sub-barrier fusion appears in the review by Reisdorf [21].

Neutron-rich nuclides are inaccessible *via* the compound nuclear reaction. To produce neutron-rich transuranium nuclides, heavy-ion-induced transfer reactions of actinide targets ranging from ^{238}U to ^{254}Es with a variety of incident particles ranging from ^{16}O to ^{238}U have been studied. A typical example of such attempts was the study of the $^{238}U + ^{238}U$ reaction at GSI (GSI Helmholtzzentrum für Schwerionenforschung, Darmstadt). In Fig. 3, the production yields of transuranium isotopes for the reaction of 7.5 MeV/u-^{238}U ions with thick ^{238}U targets are shown [22]. The yield distributions of the heavy actinides were found to show similar bell-shaped variations with the atomic number Z and mass number A as observed in the $^{238}U + ^{136}Xe$ reaction. The yields of each isotope in the $^{238}U + ^{238}U$ reaction, however, are much larger than those observed in the $^{238}U + ^{136}Xe$ reaction. Schädel *et al.* also measured the yields of heavy actinides in the reaction of ^{238}U with ^{248}Cm and the results showed that the shapes and centroids of the isotopic distributions are similar in all cases but the magnitudes of the yields are the greatest in the $^{248}Cm + ^{238}U$ reaction [23].

Interesting results were reported for the bombardments of ^{248}Cm with the ^{40}Ca, ^{44}Ca, and ^{48}Ca projectiles. Production yields for elements through Fm are shown in Fig. 4a [24]. Considerable difference is observed in the yields of the

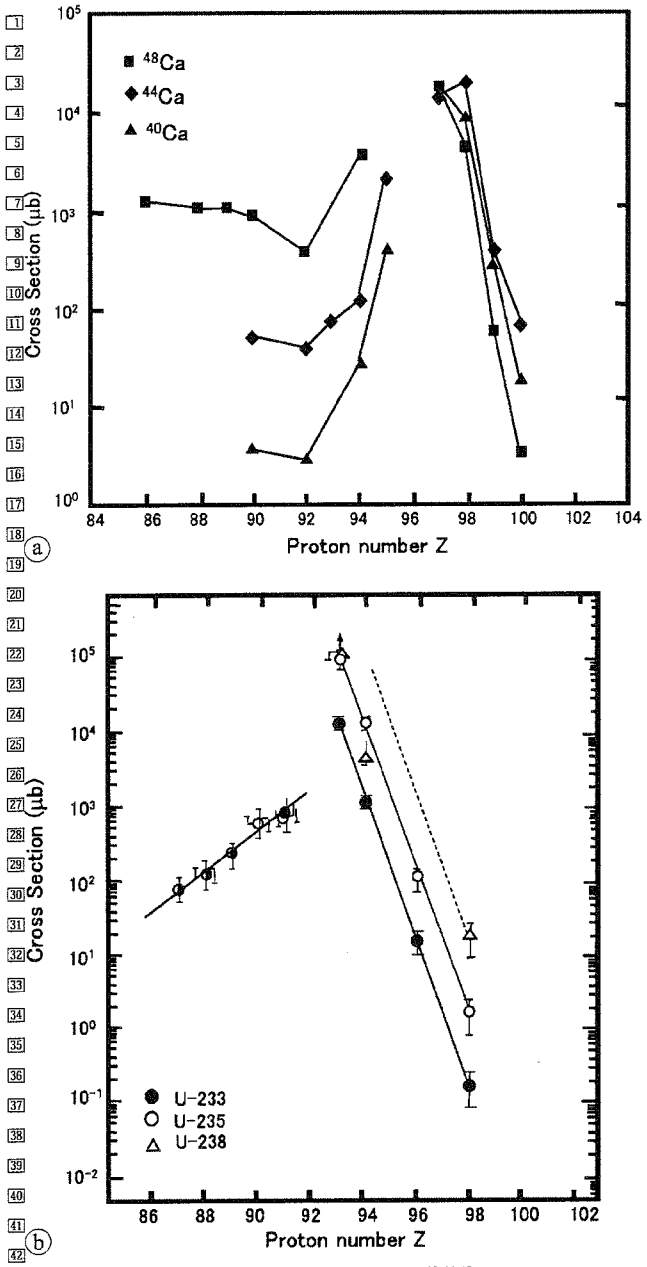

Fig. 4. (**a**) Element yields in the reactions of ^{40,44,48}Ca projectiles with ^{248}Cm [24] and (**b**) those for the ^{40}Ar + ^{233,235,238}U reactions [25].

below-target elements with the highest yields observed for ^{48}Ca, while for the above-target elements the lowest yields were observed for the ^{48}Ca projectile. The most neutron-rich nuclides in the isotopic yield distribution were observed for the reactions with ^{48}Ca. The reactions of ^{40}Ar with ^{233}U, ^{235}U, and ^{238}U were studied at the energy of the Coulomb barrier [25]. Contrary to the above ^{248}Cm + Ca reactions, the element yields below uranium are the same within the limits of errors for the three target nuclides, while the yields of the above-target elements are in the order of ^{238}U, ^{235}U and ^{233}U as shown in Fig. 4b.

Neutron-rich isotopes of heavier actinides such as ^{262}No and ^{261,262}Lr, were produced through transfer reactions by bombardments of highly radioactive ^{254}Es ($T_{1/2}$ = 275.7 d) targets with heavy ions [26]. Most recently, it is suggested that the nuclear shell structure may strongly influence the nucleon flow in the low-energy reactions with heavy ions. The production of neutron-rich heavy nuclei in the multi-nucleon transfer processes of low-energy heavy-ion collisions that are based on the dynamical multi-dimensional Langevin equation has been proposed by Zagrebaev and Greiner [27].

3.3 Experimental techniques for identification of short-lived transuranium nuclei

In the study of the mechanism of heavy-ion reaction resulting in transuranium products and for investigating nuclear properties of transuranium nuclei, it is of great importance to isolate and uniquely identify the products by their atomic number Z, mass number A and production cross sections. The claim for the discovery of a new element must present a clear evidence for unequivocal identification of Z, while that of a new isotope has to be made with the determination of both Z and A.

A review of the experimental techniques is given in several articles [28–30]. A comparison of characteristics, such as separation time and total efficiency, of various methods generally used for isolating and identifying transuranium reaction products is presented in Table 2. In the following, some typical techniques used for the study of transuranium nuclei are briefly introduced.

For studying fission properties such as mass-yield and total kinetic energy (TKE) distributions of very short-lived spontaneous fission (SF) isotopes, the SWAMI (spinning-wheel analyzer for millisecond isotopes) apparatus was constructed [31]. A portion of the recoil products emerging from the target is stopped in 100 μg/cm^2 Al foils in continuous band on the rotating disk. These foils rotate between four pairs of detectors that measure the energy deposited by correlated fission fragments when the product nuclei decay by SF. For example, SF properties of 1.2-ms ^{258}No produced through the ^{248}Cm(^{13}C, 3n) reaction was studied with SWAMI.

A gas-jet transport method is conventionally used to identify and study short-lived transuranium nuclei. Nuclei recoiling out of a target are stopped in a volume of the gas like He which is loaded with aerosols, such as KCl, PbI_2, C clusters, and MoO_3. The products attached to the aerosols are swept out of a target recoil chamber with the He gas and are transported through a capillary to a detection

Table 2. Comparison of characteristics of experimental techniques for isolating transuranium reaction products. Taken from [5].

Method	Separation time (s)	Total efficiency (%)
Rotating wheel catcher	10^{-3}	60
Gas-jet transport	10^{-1}	50
Gas-jet coupled to rapid chemical separation	10^{1}	30–40
Gas-jet coupled to ISOL[a]	10^{0}	1
Gas-filled separator	10^{-6}	25–60
Velocity separator	10^{-6}	20

a: ISOL: isotope separator on-line.

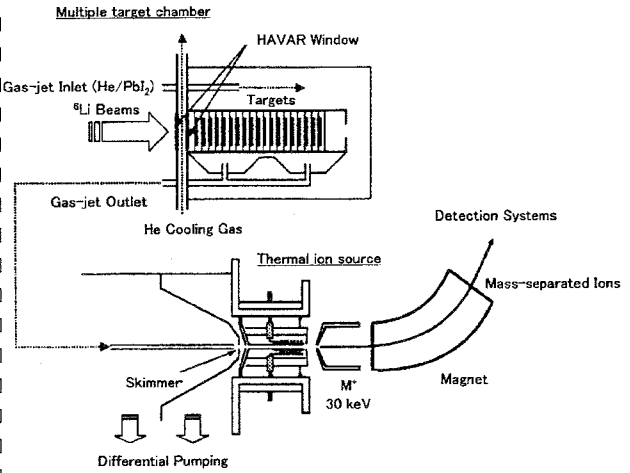

Fig. 5. Schematic view of the gas jet coupled JAEA-ISOL [32].

system or other apparatuses. To search for new transuranium nuclides and to study decay properties of these nuclei, a composite system consisting of the gas-jet transport apparatus and an on-line isotope separator (JAEA-ISOL) has been developed by Ichikawa *et al.* [32]. This system enables us to simultaneously determine the mass number *via* the isotope separator and the atomic number by the measurement of X-rays associated with the EC/β decay of a nucleus. The experimental set-up is schematically drawn in Fig. 5. Targets are mounted in a multiple target system. Reaction products recoiling from targets are thermalized in the He gas loaded with PbI_2 aerosol clusters. The products attached to the aerosols are swept out of the target chamber and transported to the thermal ion source of ISOL through the gas-jet. The transported nuclides are ionized, mass separated, and collected on an aluminum coated Mylar tape in the tape transport system or in the rotating catcher foil apparatus. The new isotope ^{241}Bk produced in the ^{239}Pu(^{6}Li, $4n$) reaction was identified by the measurement of the characteristic Cm X-rays associated with the EC decay of the nucleus separated for mass number $A = 241$ [33].

The identification of new nuclides ^{243,244}Np with the gas-jet coupled to a rapid chemical separation method [34] was conducted as follows. Chemical separation procedures were used to isolate Np from other reaction products in the ^{244}Pu + ^{136}Xe reaction. The method involved a series of solvent extractions performed continuously with the centrifuge system SISAK (Short-lived Isotopes Studied by the AKUFVE Technique) as shown in Fig. 6; reaction products were transported with the argon (Ar) gas-jet system to the chemistry laboratory. The transported products were dissolved in dilute HCl containing $TiCl_3$, which reduced Np to the 3+ oxidation state. The products of U, Th and several fission products were extracted into di (2-ethyl-hexyl) orthophosphoric acid in CCl_4 (HDEHP/CCl_4). The fraction of Np was extracted in the second HDEHP/CCl_4 step after oxidation to the 4+ state with HNO_3, and was back-extracted with phosphoric acid. Then the Np fraction was continuously pumped through a Teflon tube to the front face of a series of Ge γ-ray detectors.

The new isotope ^{253}Md produced in the ^{243}Am(^{13}C, $3n$) reaction was identified by using the Automated Chromatographic Chemical Element Separator System, ACCESS, in

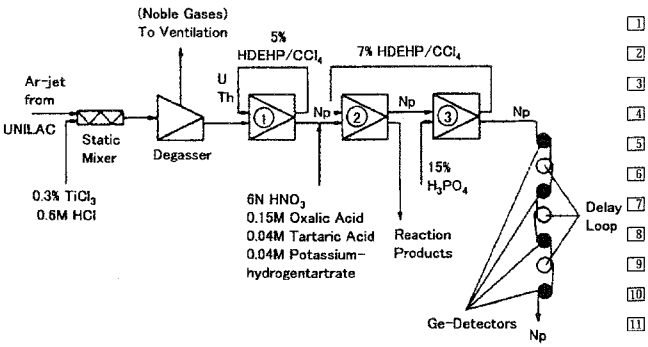

Fig. 6. Schematic diagram of the SISAK set-up used for the identification of ^{243,244}Np [35].

which ammonium α-hydroxy isobutyrate (α-HIB) was used for the separation of Md [36].

As indicated in Table 2, for detection and identification of isotopes with $T_{1/2} < 1$ ms, one has to employ in-flight separators based on electromagnetic separation of reaction products. Currently working in-flight separators for studies of transuranium nuclei are summarized in [5] and the detailed description of the in-flight separators is given by Münzenberg [37]. Part of in-flight techniques is also presented in other articles in this issue.

In the region of heavy elements, γ-ray spectroscopic studies were restricted because of the severe background arising from fission products. This problem was essentially solved by the employment of the new Recoil Decay Tagging (RDT) technique [38] that consists of an in-beam γ-ray apparatus and the recoil mass separator. The characteristic decay modes offer a signature that a particular nuclide has been produced, and can be efficiently detected by a focal plane detector behind the in-glight separator. Prompt γ rays at the target are detected by large Ge detector arrays.

As typical examples, the gas-filled recoil separator RITU (Recoil Ion Transport Unit) [39] and the recoil mass separator FMA (Fragment Mass Analyzer) [40] in conjunction with germanium (Ge) detector arrays have been used for the study of the nuclear structure in the region of No isotopes [41, 42]. RITU has been designed to separate nuclides produced through compound nuclear reactions from beam particles and other reaction products, especially fission products. To collect reaction products efficiently in the focal plane of the separator, dilute gas was filled in a dipole magnet.

3.4 Exotic nuclear properties of heavy nuclei

Decay properties of transuranium nuclides lead to the understanding of proton excess heavy nuclei: verification of the proton drip line, nuclear structure of large deformed nuclei such as octupole and hexadecapole deformation, and fission barrier heights. Recent nuclear and decay properties of nuclei in their ground – and isomeric – states are compiled and evaluated by Audi *et al.* [43], while the calculated atomic mass excess and nuclear ground-state deformations are tabulated by Möller *et al.* [44]. Calculated fission barriers for heavy elements based on the macroscopic–microscopic finite-range liquid drop model are presented in [45]. In the following, exotic nuclear decay properties of heavy nuclei are briefly introduced.

3.4.1 Nuclear structure

As described in the previous sub-section, the spectroscopic studies of the heaviest nuclei have been vigorously performed with large γ-ray detector arrays, Gammasphere [46], Jurosphere and SARI (Segmented Array at RITU) arrays [39], and the electron spectrometer SACRED (Solenoid and Array for Conversion Electron Detection) [47] coupled with the recoil separator. The recent experimental progress of nuclear structure study of the heaviest nuclei is summarized by Leino and Heßberger [48] and Herzberg [49], while theoretical description is reviewed by Sobiczewski and Pomorski [50]. As the details about the nuclear structure study are also given by Herzberg and Sobiczewski in this issue, we briefly mention about some topics in the following; α–γ and α–electron (α–e) decay spectroscopy of the neutron-rich nuclide ^{257}No produced in the ^{248}Cm(^{13}C, $4n$) reaction was carried out at JAEA using a rotating wheel detection system coupled with the gas-jet and the gas-jet transport coupled to ISOL. On the basis of the α- and γ-transition energies, α–γ, α–e, and e–e coincidence relations, the decay scheme of ^{257}No was established [51]. Enhanced stability of heavy nuclei due to high-spin isomers (K-isomers) is predicted [52]. The multi-quasi-particle configurations with high K-isomeric states have been identified in ^{254}No [42]. In-beam γ-ray spectroscopic studies of neutron-rich transuranium nuclei, ^{245,246}Pu and ^{249,250}Cm, have been conducted through the unique nucleon transfer reactions using the neutron-rich beams, such as ^{18}O. The ground-state bands of these nuclei were successfully established [53].

A high-precision mass measurement system with Penning traps, SHIPTRAP at GSI has been developed to investigate nuclear structure of rare isotopes far from stability. The direct mass measurements of $^{252-254}$No have been successfully performed [54]. Spectroscopic studies of superdeformed fission isomers have been reviewed by Bjornholm and Lynn [55], while recent progress of spectroscopy in the second and third minimum of the potential energy surface is summarized by Thirolf and Habs [56]. Krasznahorkay *et al.* succeeded to observe hyperdeformed rotational bands in actinide nuclei [57].

3.4.2 Cluster radioactivities

A charged particle heavier than an α particle but lighter than a fission fragment, such as C, O, F, Ne, Mg and Si isotopes, is spontaneously emitted in a cluster decay of a heavy nucleus. The cluster decay was first predicted by Sandulescu *et al.* [58] and experimentally discovered by Rose and Jones in the decay: $^{223}\mathrm{Ra} \rightarrow {}^{14}\mathrm{C} + {}^{209}\mathrm{Pb}$ [59]. The probability for the decay was $\sim 10^{-9}$ of the α-decay probability. The data obtained until now on half-lives and branching ratios relative to α decay are summarized in review articles [5, 60, 61].

3.4.3 Delayed fission

Delayed fission is also an exotic nuclear decay process of heavy nuclei that is observed subsequent to β/EC decay. In the delayed fission process, β decays or EC of the parent nuclide populate excited states of the daughter nucleus, and if these states are of energies comparable to or greater than the fission barrier of the daughter nucleus, then fission may compete with other decay modes of the excited states. Reviews give a detailed description of the delayed fission [62].

Delayed fission permits studies of fission properties of nuclei far from stability and γ de-excitation of nuclear levels in the second minimum of the potential energy surface. There has been also considerable theoretical interest in β-delayed fission process because it may significantly affect the final abundance of heavy elements produced in the astrophysical r-process and in other multiple neutron capture processes taking place in very high neutron flux, such as thermonuclear explosions [63]. The experimental data on the delayed fission are summarized in [5].

3.4.4 Spontaneous fission

Spontaneous fission (SF) is observed only in elements with $Z \geq 90$ where Coulomb forces make the nucleus unstable toward this mode of decay, although energetically SF is an exothermic process for nuclei with $A \geq 100$. Numerous reviews of SF properties, half-lives and properties of fission fragments, have been summarized by several authors [64–66]. Some current topics concerning SF are presented in the following.

Schematic representations of all of the measured mass-yield distributions (normalized to 200% fragment yield) for SF of the trans-Bk isotopes are shown in Fig. 7 [66]. It is interesting to observe rather sudden changes from asymmetric to symmetric fission as reflected by the mass distributions changing from asymmetric to symmetric mass distributions as the neutron number increases toward $N \approx 160$ for the elements Fm ($Z = 100$), No ($Z = 102$), and Rf ($Z = 104$).

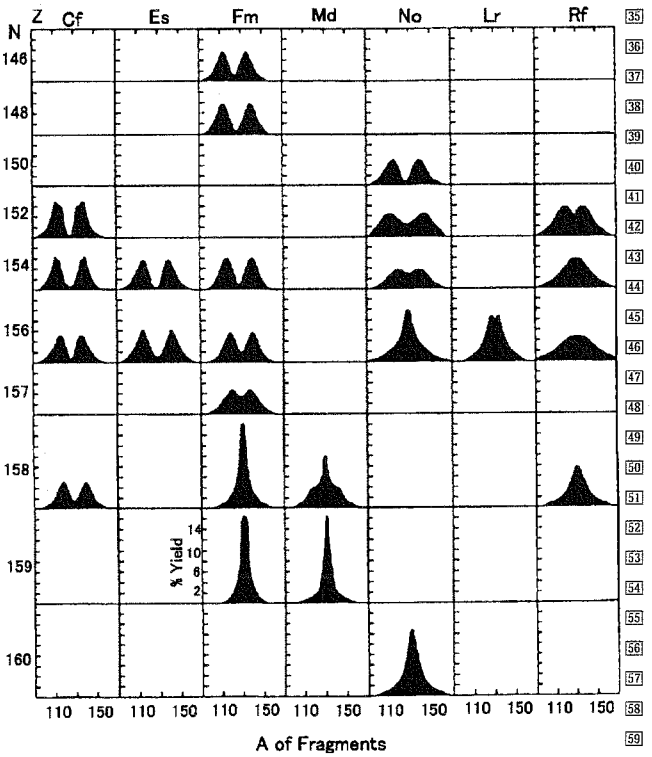

Fig. 7. Schematic representation of all known mass-yield distributions for SF of trans-Bk isotopes [63].

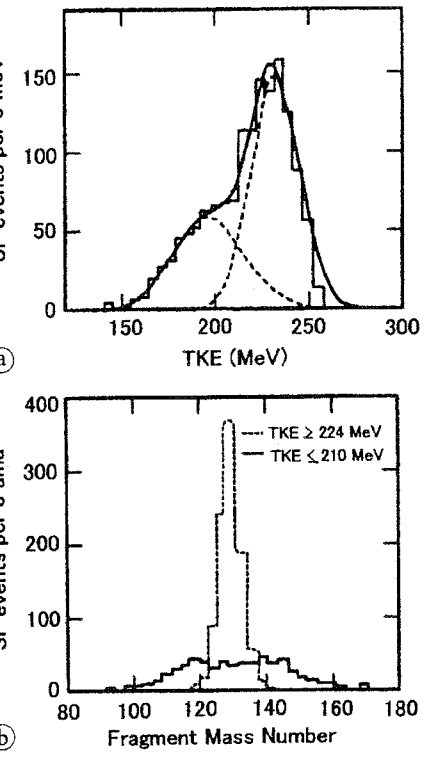

Fig. 8. (a) TKE distribution for SF of ^{260}Md. (b) Decomposed mass-yield distributions for the events with TKE $\geq$ 224 MeV (dashed histogram) and for those with TKE $\leq$ 210 MeV (solid histogram) [68].

The other interesting feature in SF of very heavy actinides is bimodal fission. The existence of two distinctively different scission configurations for the same mass division was demonstrated in SF of the heavy actinides [31, 67]. The most striking and significant features are that the mass-yield distribution is essentially single-peaked around the symmetric mass split, resulting in products with the mass number $A \approx 130$, whereas the total kinetic energy (TKE) distribution apparently exhibits the structure with a shoulder that strongly suggests the presence of at least two components in the TKE distribution. As typical data, the TKE and mass-yield distributions observed in SF of ^{260}Md [68] are depicted in Fig. 8a,b, respectively; two components are clearly seen in the TKE distribution. The two-component analysis yielded the fact that the high-TKE events mostly constitute the sharp mass-yield curve around symmetry and the low-TKE ones a broad flat-topped distribution. Some theoretical calculations to understand bimodal fission of heavy actinides have been extensively performed, such as in [69, 70].

A sudden change of the mass distribution depending on the neutron number of the fissioning nuclei was reported by Wagemans *et al.* for SF of plutonium, ^{236,238,240,242,244}Pu [71–73]. The change of neutrons among the isotopes studied yields a drastic change in the mass and TKE distributions. An attempt was made to understand the phenomena in terms of the model of multi-modal random neck rupture [74]. Recent studies of SF of ^{252}Cf with large γ-ray detector arrays, Gammasphere [46], revealed a new fission mode, cold fission with no neutron emission in the pair fragments of Zr-Ce and Mo-Ba [75]. Cold ternary SF, as $^{252}\text{Cf} \rightarrow {}^{146}\text{Ba} + {}^{96}\text{Sr} + {}^{10}\text{Be}$, has also been identified by measuring the various γ-transitions of these nuclei in coincidence [76]. The use of the high resolution triple γ-coincidence technique can provide important information on very rare events in fission.

3.4.5 Two fission modes – symmetric and asymmetric fission

The presence of two kinds of deformation paths in low energy fission of actinides has been verified by examining the correlation among saddle-point configurations, scission configurations and mass-yield distributions [77]. The first path is initiated at higher threshold energy and ends with an elongated scission configuration, giving a final mass yield curve centered around symmetric mass division and lower TKE: the symmetric fission path. In the second path, the fissioning nucleus experiences lower threshold energy. This results in a more compact scission configuration, which gives a double humped mass-yield distribution always centered around the heavy fragment mass number $A = 140$ with higher TKE: the asymmetric fission path. The above picture is well reproduced by the theoretical calculation of the potential energy surfaces by Möller *et al.* [78]; the saddle leading to the mass-symmetric division is found to be a few MeV higher than that to the mass-asymmetric division and the compact scission configuration is related to the asymmetric fission and the elongated one associated with the symmetric fission path. The clear ridge separating the two symmetric and asymmetric fission valleys is also pointed out. Systematic features of the mass-yield and TKE distributions in both symmetric and asymmetric fission depending on A and Z of fissioning nuclei are discussed in detail by Ohtsuki *et al.* [79] and Zhao *et al.* [80]. The effects of A and Z on the relative probability of taking either deformation path, and the characteristics of the final mass division phenomena and scission properties resulting from each deformation path have been extensively studied.

Elemental yields of fission fragments in the Coulomb fission have been obtained for a number of neutron-deficient actinides and preactinides by using the unique method, relativistic radioactive beams [81]. In Fig. 9a, the experimentally measured mass distributions are shown on the chart of nuclides, while the elemental yield distributions after Coulomb fission are depicted as functions of Z and N of the fissioning nuclei in Fig. 9b. The transition from a single-humped mass-yield distribution at ^{221}Ac to a double-humped one at ^{234}U is clearly seen. In the transition region around ^{227}Th, triple-humped distributions appear, demonstrating comparable yields for the symmetric and asymmetric fission modes.

4. Chemical properties of transuranium elements

Seaborg proposed actinide concept as an extension of the periodic table by placing a new series of transition metals below the lanthanide series [4, 82]. The actinide elements are 5 f transition elements having partly filled f and d orbitals in the valence states.

4.1 Oxidation states and ionic radii

As shown in Fig. 10, the light actinide ions, Np, Pu and Am can behave as 3+ to 7+ cations and the most stable oxi-

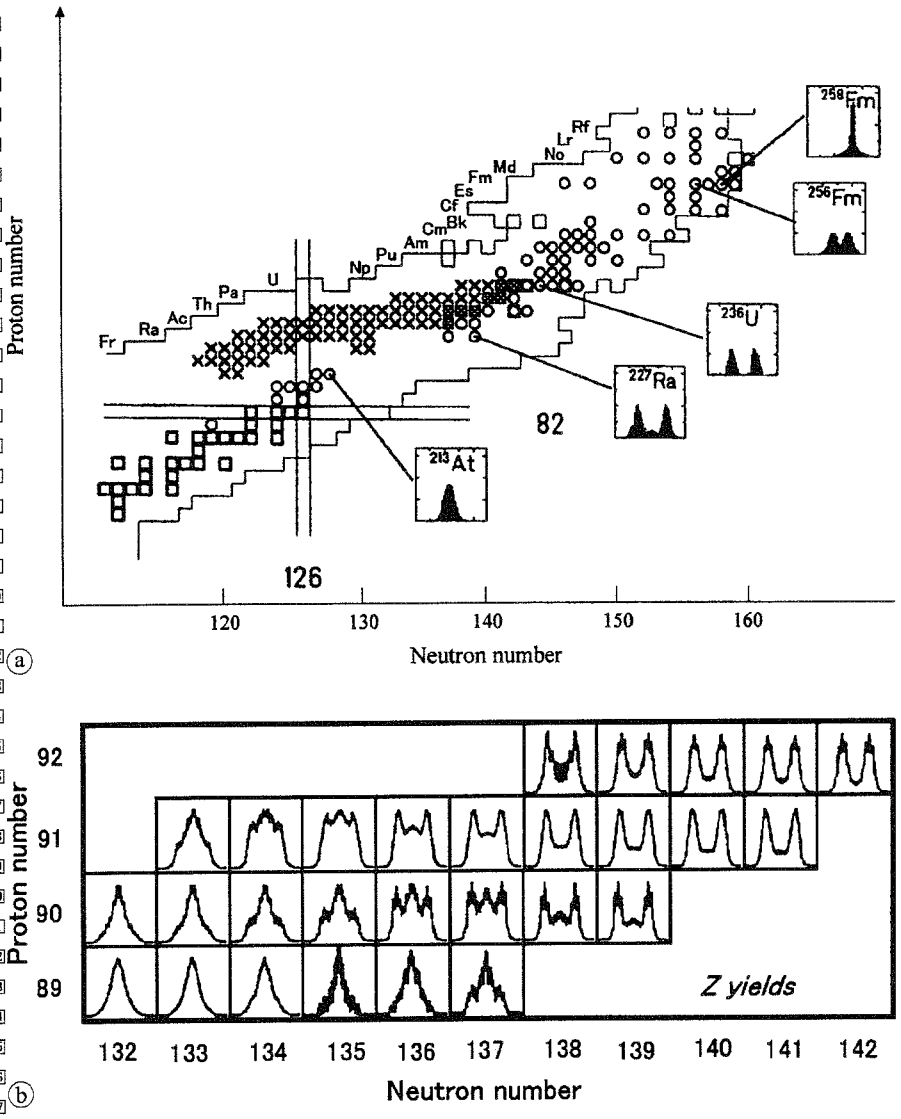

Fig. 9. (**a**) Isotopes investigated in low-energy fission are indicated on the chart of nuclides. Circles: Mass distributions measured for excitation energies less than 10 MeV above the fission barrier and those from SF. Crosses: Data obtained using the Coulomb fission by using the relativistic radioactive beams. (**b**) Fission-fragment elemental yield distributions in the range $Z = 24$ to 65 observed in Coulomb fission are shown on the chart of nuclides [81].

dation states of these three elements are 5+, 4+, and 3+, respectively [2]. Pentavalent and hexavalent actinide ions form oxygenated actinyl ions AnO_2^+ and AnO_2^{2+}. The structural information of the actinyl ions are indispensable to understand the chemical behavior of these ions, especially for the separation chemistry, the modification of reprocessing scheme, development of new extractants for actinide separation and management of the waste containing these actinides.

Table 3 gives ionic radii of lanthanide and actinide elements [2]. Marcus publised the data book on the properties of ions including actinides [83]. Ionic radii decreases with increasing atomic number and this tendency is called actinide contraction. The ionic radii are one of the useful information to understand the behavior of actinide ions. Because of the actinide contraction, the effective charge of heavy trivalent actinide ions are relatively larger than those of the lighter ones.

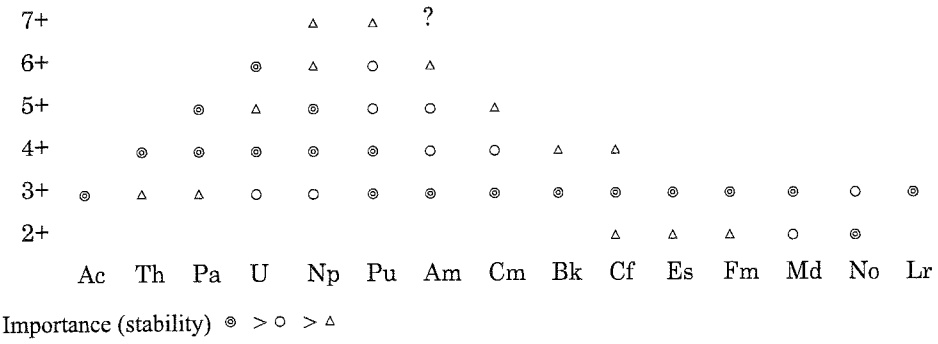

Fig. 10. Oxidation states of actinide ions.

Table 3. Ionic radii of lanthanide and actinide elements [1, 83[a], 84[b]].

Z	Element	Ln^{3+} (nm)	Ln^{4+} (nm)	Z	Element	An^{3+} (nm)	An^{4+} (nm)
57	La	0.1061		89	Ac	0.1119	
58	Ce	0.1034	0.092	90	Th	(0.108)	0.0972
59	Pr	0.1013	0.090	91	Pa	(0.105)	0.0935
60	Nd	0.0995		92	U	0.1041	0.0918
61	Pm	(0.0979)		93	Np	0.1017	0.0903
62	Sm	0.0964		94	Pu	0.0997	0.0887
63	Eu	0.0950		95	Am	0.0982	0.0878
64	Gd	0.0938		96	Cm	0.0970	0.0871
65	Tb	0.0923	0.084	97	Bk	0.0949	0.0860
66	Dy	0.0908		98	Cf	0.0934	0.0851
67	Ho	0.0894		99	Es	0.0925	
68	Er	0.0881		100	Fm	–	
69	Tm	0.0869		101	Md	0.0896[a]	
70	Yb	0.0858		102	No	0.0894[b]	
71	Lu	0.0848		103	Lr	0.0882[a]	

4.2 Promotion energies of the actinide series

The 5 *f* transition elements, actinides, have wider *f* orbital radial distribution compared with that of the 4 *f* transition elements, lanthanides. Since the chemical behavior of elements is characterized by the configuration of valence electrons, the 5 *f* and 6*d* states are the factors in determining their physical and chemical properties. The function of these valence electrons can be changed by environment, for example, pressure, temperature, and chemical interaction.

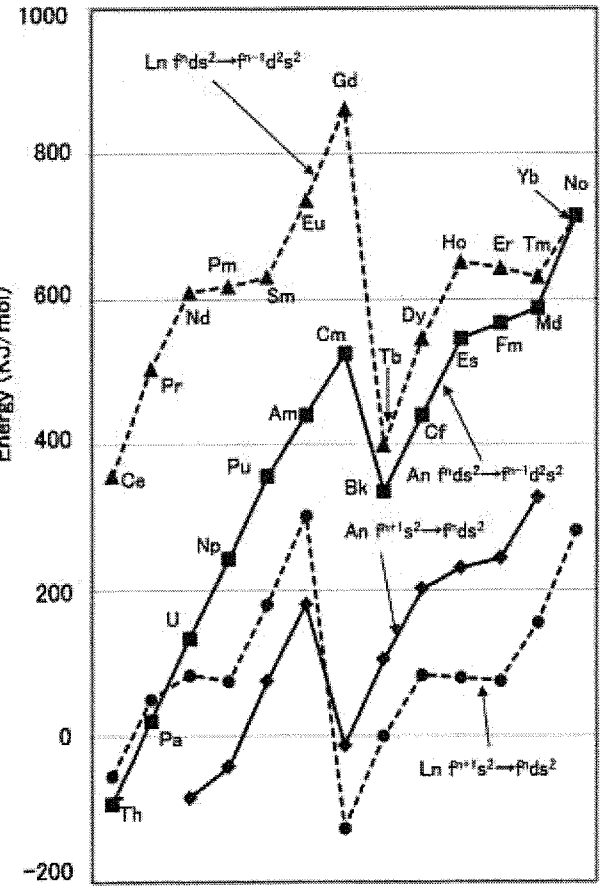

Fig. 11. Promotion energies for $f \rightarrow d$ conversion in the lanthanides and actinides series.

Fig. 11 shows $f \rightarrow d$ promotion energies for lanthanides and actinides [86]. The $f \rightarrow d$ promotion energy means required energy to excite an *f* electron to a *d* orbital. To discuss the physical and chemical properties of actinides, $f \rightarrow d$ promotion energy must be fundamental information to grasp the 5 *f* electron contribution to the chemical interaction. In Fig. 11, the energy difference between Ln(An) $f^n ds^2$ and $f^{n-1} d^2 s^2$ indicates the stability of the $Ln(An)^{4+}$ to $Ln(An)^{3+}$ states. The energy difference plots of Ln(An) $f^{n+1} s^2 \rightarrow f^n ds^2$ also indicates the relative stability of the $Ln(An)^{3+}$ states to the $Ln(An)^{2+}$ states.

The Ln $f^n ds^2 \rightarrow f^{n-1} d^2 s^2$ energies for lanthanides are higher than those of the actinide series, therefore the Ln^{3+} state is more stable than the Ln^{4+} states. The $f^{n+1} s^2 \rightarrow f^n ds^2$ promotion energies of the lighter lanthanides are higher than the actinides, while for the heavier lanthanides (from Gd to Yb), the promotion energies are smaller than those of the actinides. The promotion energy of $5f \rightarrow 6d$ for the lighter actinides is relatively smaller than that of $4f \rightarrow 5d$ of the lanthanides. This means that the 5 *f* electrons of lighter actinides are more chemically active than the corresponding 4 *f* electrons in the lanthanides. The trivalent state becomes more stable above americium in acidic solution like corresponding lanthanides. One of the interesting elements in the heavy actinides is nobelium (No), $Z = 102$, because the divalent state is stable in acidic condition.

Generally, we can sort out the actinides into two groups for descriptive purposes. Group 1 is the lighter actinides from Th to Cm which are of interest for nuclear industrial application and the other heavier actinides group is of interest for basic science of heavy elements. Th, U, and Pu are for nuclear fuels and Np, Am, and Cm are treated as radiotoxic long-lived minor actinides (MA).

As there are several review papers and books on the chemistry of transuranium elements [1, 2, 5], we briefly summarize recent advances in chemistry of these transuranium elements in this section.

4.3 Solution and separation chemistry of transuranium elements

In an acidic condition, actinide ions from Am to Lr take 3+ as the most stable oxidation state and they behave like the

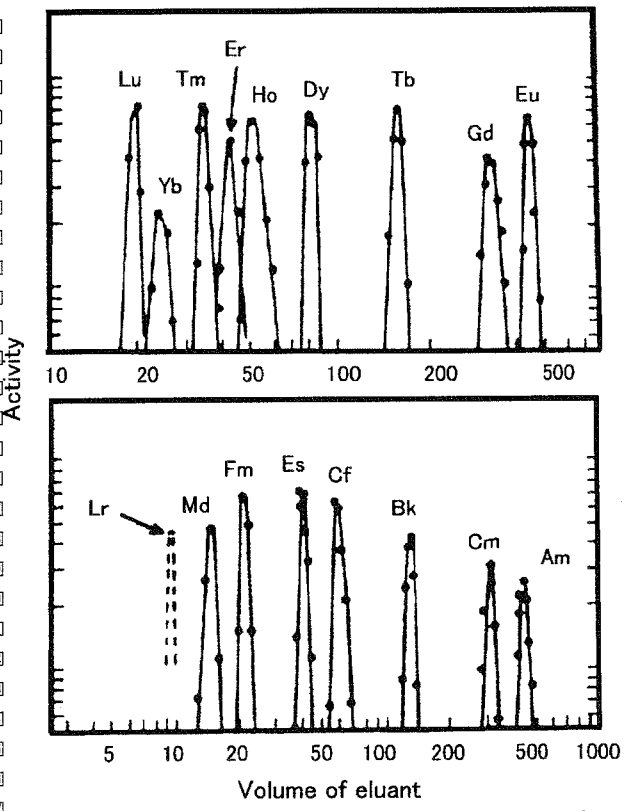

Fig. 12. Elution curves for 3+ lanthanide and actinide ions from Dowex-50 ion-exchange resin with ammonium α-hydroxy-isobutyrate eluent.

lanthanide ions, except for No which seems to prefer the 2+ state. Fig. 12 shows elution curves for lanthanide and actinide ions from a cation-exchange column. The elements above fermium must be produced in accelerators and are available in quantities of several atoms at a time. The frequent chemical identification of heavy actinide ions was carried out by eluting the ions from cation exchange columns. The elution pattern of lanthanide ions made it possible to predict the expected elution position for new trivalent actinide ions, because the ionic radii of trivalent actinide ions decrease with increasing the atomic number. Brüchle *et al.* estimated ionic radii of Md^{3+} and Lr^{3+} on the basis of cation-exchange chromatography and additionally they calculated the hydration enthalpies of these actinide ions by using the Born–Haber cycle [87].

One of the interesting subjects of heavy actinides is the chemistry of the No ion. The electron configuration of No is [Rn]5$f^{14}7s^2$. Because of the strong stability of the 5f^{14} closed shell, No behaves as the 2+ ion in solution. Toyoshima *et al.* [88] applied the electrochemical technique to oxidize No^{2+} to No^{3+} and succeeded to estimate the formal redox potential of [$No^{3+} + e^- \rightleftarrows No^{2+}$] to be 0.75 V.

4.3.1 Structural chemistry of actinide ions

A XAFS (X-ray absorption fine structure) technique is widely applied to the solution chemistry of actinides that is generally divided into the two techniques: XANES (X-ray absorption near edge structure) and EXAFS (Extended X-ray absorption fine structure). XANES is associated with the excitation process of a core electron to bound and quasi-bound states. Meanwhile, EXAFS is an oscillatory structure observed over the wide energy range just above the XANES region.

Antonio *et al.* [89] studied Np redox properties by an *in-situ* EXAFS and performed density functional theory (DFT) calculations. They reported structural change of coordinated oxygen to Np for the Np^{3+}/Np^{4+} and NpO_2^{2+}/NpO_2^+ couples and confirmed the hydration of NpO_2^+ and NpO_2^{2+} is the same with 5 equatorial water molecules. Kitatuji *et al.* investigated redox behavior of Np ions by controlled potential electrolysis and voltammetry techniques [90]. They determined the electrochemical reduction mechanism of NpO_2^+ to Np^{4+} or Np^{3+}. Ikeda and Hennig *et al.* [91] carried out EXAFS study of Np in perchlorate and nitrate solution at European Synchrotron Radiation Facility (ESRF) in combination with cyclic voltammetry. The electrochemical reaction of the NpO_2^{2+}/NpO_2^+ couple involves the extension of interatomic distance between Np and the coordinated atoms, resulting from the net charge decrease of the Np atom. The XAFS study of complex formation of neptunyl acetates is also reported by Takao *et al.* [92]. They measured stability constants of several NpO_2^+ acetate complexes by UV-vis-NIR titration and determined the coordination structure of acetates to the NpO_2^+.

Structural chemistry of Pu solution is widely investigated by Conradson and his colleagues [93]. More than 60 Pu L_3 X-ray absorption spectra are reported for hydrates, nitrates, chlorides, and other compounds. Their article is a useful database to find the XANES structure of various oxidation states of the Pu ions.

The sorption behavior of Am^{3+} onto 6-line-ferrihydrite was studied using EXAFS at the ESRF by Stumpf *et al.* [94]. They obtained EXAFS signals both at pH 5.5 and at pH 8.0 and well explained the difference of sorption behavior of Am^{3+} by changing the pH value. Denecke *et al.* [95] investigated coordination structure of Cm^{3+} and Eu^{3+} with the *N*-donor ligand, the 2,6-di(5,6-dipropyl-1,2,4-triazin-3-yl) pyridine (BTP) ligand using EXAFS, time-resolved laser fluorescence spectroscopy (TRFLS), and quantum chemical calculations. The BTP ligand is one of the promising extractants for these trivalent MA separations from the lanthanides, so that this kind of research is key issue to understand the chemical bonding of Cm^{3+} with the ligands.

Hydration structure of trivalent californium (Cf^{3+}) is reported by Galbis *et al.* [96] for the first time using the EXAFS method and theoretical evaluation by the DFT method. They conducted the experiments using a limited amount of ^{249}Cf with the half-life of 351 y. Apostolidis *et al.* [97] also reported structures of $An(H_2O)_9(CF_3SO_3)_3$ of U–Cm and Cf with UV/Vis/NIR spectroscopy, crystallography and theoretical DFT calculations. They compared An–O distances with experiments and several levels of DFT calculations and additionally they predicted the hydration structure of Bk.

The XAFS research is, in many cases, conducted coupled with computational techniques, molecular dynamics simulations, or DFT calculations, because EXAFS information is only limited to the one dimensional distance and the determination of coordination number includes uncertainties of 20% [98]. For this reason, computer simulations are helpful

to compensate the experimental uncertainties. Denecke reviewed the XAFS application to the actinide speciation that is available to figure out the actinide structural chemistry by the X-ray absorption technique [99]. Computational studies of the actinide solution chemistry are mainly carried out by the application of Gaussian program package [100] with the Effective core potential for the actinides and the Amsterdam Density Functional (ADF) program package [101] with zeroth order relativistic approximation (ZORA) Hamiltonian for Scalar relativistic calculations. Shamov and Schreckenbach [102] applied the small-core potentials formalism to the hydration structure studies of actinide complexes, and Hay *et al.* [103] reported the structure of $[AnO_2(OH_2)_5]^{n+}$, (An = U, Np, or Pu, $n = 1$ or 2) and the stability analysis of neptunium (VII) in alkaline solutions, $[NpO_2(OH)_4]^{1-}$ and $[NpO_4(OH)_2]^{3-}$.

4.3.2 Separation chemistry of actinide ions

According to the Pearson's HSAB (Hard Soft Acid Base) theory [104], oxygen is considered to be a typical hard donor, whereas nitrogen and sulfur are softer than oxygen. The HSAB theory is available for the computational design for the extractant molecule of MA separation because the information related to HSAB strongly related to the energy levels of HOMO of the donor atoms of ligands and LUMO of the cations.

4.3.3 Oxygen donor extractants

In 1980's, Horwitz *et al.* [105, 106] created a boom of MA separation research with subsequent development of P=O based extractants, CMP (R_1R_2-*N,N*-di(R′) carbamoylmethyl phosphonate) and CMPO (R_1R_2-*N,N*,-di(R′)-carbamoylmethyl phosphine oxide). In the CMPO system, Am is preferentially extracted with thiocyanate as a counter ion and the separation factor (S.F.) (Am^{3+}/Eu^{3+}) is about 7 [107]. They proposed the TRUEX (Trans Uranium Extraction) process for the TRU extraction separation scheme by using the CMPO compounds. In this process, CMPO extracts trivalent actinide ions from the waste solution from the PUREX process, while the stripping process is practically difficult because of its higher coordinating ability.

Sasaki and *et al.* investigated the separation scheme by using newly developed C=O donor extractant TODGA (*N,N,N′,N′*-tetraoctyl diglycoleamide) (see Fig. 13) for the trivalent actinides recovery from a raffinate solution of PUREX reprocessing waste [108, 109].

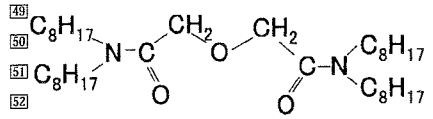

Fig. 13. Structure of TODGA molecule.

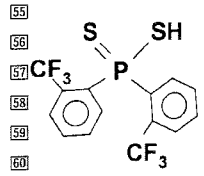

Fig. 14. Structure of bis(*o*-trifluoromethylphenyl) DPAH.

They reported the distribution ratios (D_M) of lanthanide and actinide ions and compared the D_M values with that of Am^{3+} in the extraction system of 1 M HNO_3 and 0.1 M TODGA/*n*-dodecane. The order of extractability of actinide ions from 1 M HNO_3 is An^{3+}, $An^{4+} > AnO_2^{2+} > AnO_2^{+}$. The TODGA has an ability of co-extraction of trivalent actinide ions and lanthanide ions from high-level liquid radioactive waste and is suitable for the mutual separation between trivalent actinide ions and the AnO_2^{2+}, AnO_2^{+} ions. Ansari *et al.* applied the TODGA molecule to the separation process of MAs from high level liquid waste using a hollow-fiber supported liquid membrane [110].

4.3.4 Sulfur donor extractants

For the mutual separation between trivalent actinide ions and lanthanide ions, soft donor extractants containing sulfur and/or nitrogen donors were widely investigated. As extractant contains the P=S group in the molecule, the sulfur atom has potential for selective coordination to Am^{3+} and Cm^{3+} against the trivalent lanthanide ions. The sulfur type soft donor extractant, thiophosphoric acid is a candidate for selective separation of trivalent actinide ions from lanthanides [111]. Zhu *et al.* [112, 113] developed a dithiophosphinic acid type extractant, Cyanex-301 (bis(2,4,4-trimethylpentyl) dithiophosphinic acid), to separate selectively trivalent actinide ions from the lanthanides. They reported the average separation factor of Am^{3+} against Ln^{3+} being greater than 2300. Chen *et al.* [114] reported that the equilibrium constant for the liquid–liquid extraction of Am^{3+} by Cyanex-301 is 5900 times larger than that of Eu^{3+}, the homologous lanthanide. In this Cyanex process, the raffinate solution must be adjusted to a pH 3 to 4. Since the Cyanex molecule is not stable in an acidic condition, there are several important subjects to solve for the industrial application of this Cyanex ligands. Klaehn *et al.* newly developed dithiophosphinic acid type extractants for MA separations. One of the aromatic type ditiophosphinic acids (R2PS2H: DPAH), bis(*o*-trifluoro methylphenyl) DPAH (Fig. 14) can selectively separate Am^{3+} from Eu^{3+} with separation factors of ~ 100 000 at low pH region [115].

To explain the difference of affinity, Cao and Dolg *et al.* [116] investigated theoretically the mechanism of Am^{3+} and Cm^{3+} separation from Eu^{3+} with Cyanex-301 type ligands. They applied DFT using the second-order Møller–Plesset perturbation theory with the conductor-like screening model (COSMO) approach. The calculated Gibbs free energy difference in the extraction reaction agreed well with the thermodynamical property for Am^{3+} and Cm^{3+}.

4.3.5 Nitrogen donor extractants

Kolarik *et al.* [117, 118] and Madic *et al.* [119] carried out comprehensive study of the separation of trivalent actinide ions from lanthanides by the nitrogen donor extractants. They developed several new nitrogen polydentate ligands, BTP [2,6-bis(5,6-dialkyl-1,2,4-triazin-3-yl)-4-alkyl-pyridines] and BTBP [6,6′-bis-(5,6-diethyl-[1,2,4]triazin-3-yl)-2,2′-bipyridyl]. They used a computational approach for molecular design of extractants and to find out the separation mechanism. Guillaumont [120] reported the An^{3+} and Ln^{3+} complexes with nitrogen donor ligands and she tried

to understand the chemical bonding between the cations and donor atoms. Although the BTP type extractants have potential for the selective separation of the An^{3+} group, they are not stable against oxidation, acidic hydrolysis, and radiolysis [121]. Drew and co-workers [122] applied BTBP/1,1,2,2-tetrachloroethane to the Am^{3+}/Eu^{3+} separation from 1 M HNO_3, and reported exceptional S.F. $(Am^{3+}/Eu^{3+}) > 160$.

4.4 Solid state properties of transuranium compounds

As discussed in the Sect. 4.1, the itinerant 5 *f* electrons of lighter actinides strongly contribute to the chemical bonding in the metallic phases, alloys, and other solid state compounds, while the heavier actinides having localized 5 *f* electrons behave like lanthanides. High pressure is the most efficient and cleanest way of changing the interatomic distances in a lattice. The changing the interatomic distance should affect the bonding and electron configurations so that many experiments are conducted to explore the role of 5 *f* electrons combined with the computational approach [123].

In this sub-section, we briefly summarize recent activities of basic research on the metals and alloys of actinides and several important progresses of nuclear fuel technologies including oxides and nitrides.

4.4.1 High pressure study of actinide alloys

Fig. 15 shows atomic volumes of lanthanide and actinide metals. The lighter actinide metals from Pa to Pu take smaller atomic volumes and higher densities compared with those of the heavier actinides. The metallic bonding becomes stronger by the contribution of 5 *f* electrons in the lighter actinide metals. The atomic volume of Am is relatively larger than those of U, Np, and Pu and several references provide details concerning the structural change of Am metal under high pressure [124–127].

The first high pressure study of Am was carried out by Stephens *et al.* [124] in 1968. They determined the compressibility and electrical resistance of Am metal. In 1980, Skriver and co-workers [125] applied the X-ray diffraction technique to the high pressure study of Am, and Benedict *et al.* conducted the experiments on phase transitions of Am under high pressure and determined the 5 *f* electron delocalization occurs at 23 GPa. Benedict [126, 127] reviewed the study of pressure-induced structural transitions in the actinide metals. Heathman, Lindbaum and co-workers [128, 129] investigated pressure induced structural change of Am by using synchrotron radiation and determined the structural behavior up to 100 GPa and they confirmed the delocalization of 5 *f* electrons by the pressure induction. Söderlind and Landa [130] investigated the crystal structural transformation of Am under high pressure theoretically by the first principle DFT method. Moore *et al.* [131] applied electron energy-loss spectroscopy (EELS) and DFT calculation to the analysis of magnetic stabilization of Cm.

The boundary of localization and delocalization transition in Pu is investigated by Marianetti *et al.* [132]. They applied the dynamical mean-field theory (DMFT) to calculate the magnetic susceptibility, heat capacity, and the temperature dependence of the valence band photoemission spectra for δ-phase plutonium (δ-Pu). The combination of DFT and DMFT is suitable for the precise evaluation of these solid state properties of the actinides. The behavior of 5 *f* electrons of the actinides is in between the more localized 4 *f* electrons of the lanthanides and the itinerant *d* electrons of the transition metals.

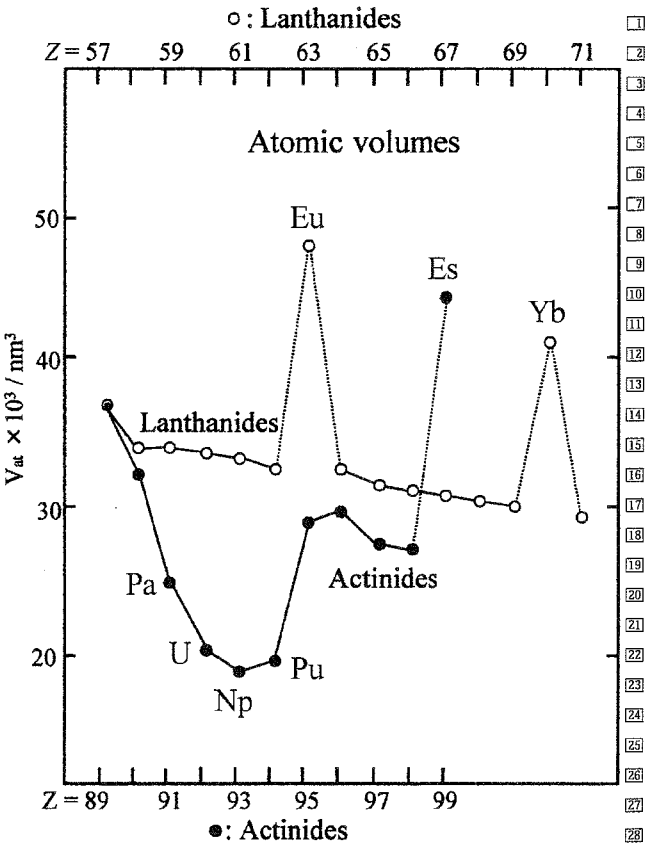

Fig. 15. Atomic volumes of lanthanide and actinide metals. Pa, U, Np, and Pu: density increased by 5 *f* bonding. Low density of Eu, Es, and Yb is due to divalency.

4.4.2 Basic study of actinide solid state compounds

The first principle calculations of solid state actinide compounds have progressed rapidly in recent years. The ground state electronic structures of AnO, An_2O_3, and AnO_2 (An = U, Np, Pu, Am, Cm, Bk and Cf) are investigated by Petit and co-workers [133]. Wang *et al.* [134] applied local density approximation (LDA) with Hubbard U parameter method, LDA + U and generalized gradient approximation (GGA), GGA + U for the electronic structure of NpO_2 and compared the phonon-dispersion curves. They compared with the stability of 5 *f* electrons with the localization-delocalization trend.

Tokunaga and his colleague [135] carried out the ^{17}O NMR study on AmO_2 and they confirmed the phase transition at 8.5 K and compared it with those of UO_2 and NpO_2. The review paper of Walstedt *et al.* [136] is available for the NMR application to the superconductivity research of actinide alloys and compounds.

Since the 1950's, superconductivity of the actinide alloys and compounds has been explored by several pioneers in

this research field [137, 138]. Sarrao *et al.* [139] discovered superconductivity in Pu based alloy, $PuCoGa_5$ having the transition temperature $T_c = 18.5$ K. The T_c of this compound is an order of magnitude greater than that is the former U and Ce based heavy-fermion systems. Curro and co-workers [140] measured nuclear spin-lattice relaxation rate and Knight shift of $PuCoGa_5$ and found the unconventional superconductivity in this alloy. $AnPd_5Al_2$ type alloys are widely investigated as a heavy-fermion superconductor. Aoki and co-workers synthesized a novel superconductor, $NpPd_5Al_2$, and confirmed the *d*-wave type superconductivity [141]. Yamagami *et al.* [142] investigated the Fermi surface structure of $NpPd_5Al_2$ by the relativistic linear-augmented-plane-wave (RLAPW) band calculation with LDA approximation. They computed the Fermi energy of $NpPd_5Al_2$ and it locates on the narrow $5f$ band width. The research on the heavy-fermion superconductors is summarized in the review article of Monthoux *et al.* [143].

The LDA level of calculation for actinide oxides is not well reproduced with the experimental results of the energy position of $5f$ electrons near the Fermi level, E_F. In order to correct this difference, an additional on-site Coulomb interaction parameter U is added for the calculation. The LDA + U method is now popular for the calculation of actinide systems. This U parameter, however, is a kind of empirical parameter and modification of this part is needed for the development of real first principle calculation for actinide solid materials. In order to improve the uncertainty of the LDA + U method, the dynamical mean-field theory (DMFT) has been proposed and well succeeded in the prediction and assignment of phonon calculations of δ-Pu [144]. Shim *et al.* [145] well reproduced the photoemission spectra of δ-Pu and confirmed the reliability of the DMFT approach.

4.4.3 Nuclear fuels and related topics

A general overview of recent progress in nuclear fuel technology was extensively reviewed by Olander [146]. He reviewed the activities and notable research topics related to nuclear fuels, including uranium and plutonium mixed oxide (MOX), pyrochemistry and reprocessing technology. This report is quite useful to grasp the status of R&D in the field of nuclear fuel technology. The R&D activities of nuclear fuels including MAs are surveyed and published by IAEA [147]. The significant topics of MA bearing fuel may be the transmutation technique in a sodium cooled fast reactors and accelerator-driven system (ADS). This report contains physical and chemical properties of MA oxides, nitrides, and alloys *etc.* Comprehensive data of the phase diagrams of binary actinide alloys are available in the book of Kassner and Peterson [148].

Recently, Havela *et al.* [149] carried out photoelectron spectroscopy of the Pu metal and Espinosa *et al.* [150] reported XAFS study of the local atomic structure of α-phase plutonium (α-Pu). Allen and co-workers [151] examined local structures of Ga-stabilized δ-Pu and Söderlind *et al.* [152] investigated electronic structure of δ-Pu by all-electron full potential linear muffin-tin orbitals (FPLMTO), Korringa–Kohn–Rostoker (KKR) and projector augmented wave (PAW) methods. Savrasov and his colleagues correctly predicted the behavior of Pu metal by the dynamical mean-field theory (DMFT) [153, 154].

A huge amount of research has been done on the oxide compounds of transuranium elements. The oxygen to metal ratio (O/M ratio) is one of the important parameters to understand the solid-state behavior of these oxides. The fluorite-structure dioxide is well studied in the research of actinide oxides. Np takes pentavalent oxide Np_2O_5, while the other transuranium elements take between the trivalent and tetravalent states in the oxides. The chemical forms of these oxides give important information on properties of irradiated nuclear fuels and solidified high-level nuclear wastes. Basic research of MA behavior is motivated to understand the redox properties of transmutation fuels in order to mitigate the oxidation of cladding tube by released oxygen from the fuels. Nishi *et al.* [155] applied the XAFS technique to the americium oxides, AmO_2 and Am_2O_3. They clearly confirmed the chemical shift of the white line energy between Am^{4+} and Am^{3+} in the oxides. Martin *et al.* also applied XAFS to the structural phase transition in the americium zirconate pyrochlore, $Am_2Zr_2O_7$ [156]. This system is one of the candidates for inert matrix target materials for the transmutation of MAs.

References

1. Seaborg, G. T., Loveland, W.: *The Elements Beyond Uranium.* John Wiley and Sons, Inc., New York (1990).
2. Morss, L. R., Edelstein, N. M., Fuger, J., Katz, J. J.: *The Chemistry of the Actinide and Transactinide Elements.* 3rd Edn., Springer, Dordrecht (2006).
3. Hofmann, S.: *On Beyond Uranium – Journey to the End of the Periodic Table.* Taylor & Francis, London (2002).
4. Seaborg, G. T.: Chem. Eng. News **23**, 2190 (1945).
5. Nagame, Y., Hirata, M., Nakahara, H.: Production and chemistry of transuranium elements. In: *Handbook of Nuclear Chemistry, Vol. 2.* (Vértes, A., Nagy, S., Klencsár, Z., eds.) Kluwer Academic Publishers, Dordrecht (2003).
6. Barber, R. C., Greenwood, N. N., Hrynkiewicz, A. Z., Jeannin, Y. P., Lefrot, M., Sakai, M., Ulehla, I., Wapstra, A. H., Wilkinson, D. H.: Prog. Part. Nucl. Phys. **29**, 453 (1992).
7. McMillan, E. M., Abelson, P. A.: Phys. Rev. **57**, 1185 (1940).
8. Seaborg, G. T., McMillan, E. M., Kennedy, J. W., Whal, A. C.: Phys. Rev. **69**, 366 (1946).
9. Ghiorso, A., James, R. A., Morgan, L. O., Seaborg, G. T.: Phys. Rev. **78**, 472 (1950).
10. Thompson, S. G., Ghiorso, A., Seaborg, G. T.: Phys. Rev. **77**, 838 (1950).
11. Thompson, S. G., Street Jr., K., Ghiorso, A., Seaborg, G. T.: Phys. Rev. **78**, 298 (1950).
12. Ghiorso, A., Thompson, S. G., Higgins, G. H., Seaborg, G. T., Studier, M. H., Fields, P. R., Fried, S. M., Diamond, H., Mech, J. F., Pyle, G. L., *et al.*: Phys. Rev. **99**, 1048 (1955).
13. Ghiorso, A., Harvey, B. G., Choppin, G. R., Thompson, S. G., Seaborg, G. T.: Phys. Rev. **98**, 1518 (1955).
14. Ghiorso, A., Sikkeland, T., Walton, J. R., Seaborg, G. T.: Phys. Rev. Lett. **1**, 18 (1958).
15. Maly, J., Sikkeland, T., Silva, R., Ghiorso, A.: Science **160**, 1114 (1968).
16. Ghiorso, A., Sikkeland, T., Larsh, A. E., Latimer, R. M.: Phys. Rev. Lett. **6**, 473 (1961).
17. Donets, E. D., Shchegolev, V. A., Ermakov, V. A.: Sov. J. At. Energy **19**, 995 (1965).
18. Silva, R., Sikkeland, T., Nurmia, M., Ghiorso, A.: Inorg. Nucl. Chem. Lett. **6**, 733 (1970).
19. Oganessian, Yu. Ts.: J. Phys. G: Nucl. Part. Phys. **34**, R165 (2007).

20. Armbruster, P.: Rep. Prog. Phys. **62**, 465 (1999).
21. Reisdorf, W.: J. Phys. G: Nucl. Part. Phys. **20**, 1297 (1994).
22. Schädel, M., Kratz, J. V., Ahrens, H., Brüchle, W., Franz, G., Gäggeler, H., Warnecke, I., Wirth, G., Herrmann, G., Trautmann, N., *et al.*: Phys. Rev. Lett. **41**, 469 (1978).
23. Schädel, M., Brüchle, W., Gäggeler, H., Kratz, J. V., Sümmerer, K., Wirth, G., Herrmann, G., Stakemann, R., Tittel, G., Trautmann, N., *et al.*: Phys. Rev. Lett. **48**, 852 (1982).
24. Türler, A., von Gunten, H. R., Leyba, J. D., Hoffman, D. C., Lee, D. M., Gregorich, K. E., Bennett, D. A., Chasteler, R. M., Gannett, C. M., Hall, H. L., *et al.*: Phys. Rev. C **46**, 1364 (1992).
25. Scherer, U. W., Brüchle, W., Brügger, M., Frink, C., Gäggeler, H., Herrmann, G., Kratz, J. V., Moody, K., Schädel, M., Sümmerer, K., *et al.*: Z. Phys. A **335**, 421 (1990).
26. Lougheed, R. W., Hulet, E. K., Wild, J. F., Moody, K. J., Dougan, R. J., Gannett, C. M., Henderson, R. A., Hoffman, D. C., Lee, D. M.: The discovery and spontaneous fission of properties of ^{262}No. In: *Proceedings of 50 Years with Nuclear Fission.* National Academy of Sciences, Washington, D. C., and National Institute of Standards and Technology Gaithersburg, MD, Vol. II, American Nuclear Society, La Grange Park, IL (1989), p. 694.
27. Zagrebaev, V., Oganessian, Yu. Ts., Itkis, M. G., Greiner, W.: Phys. Rev. C **73**, 031602 (2006).
28. Herrmann, G., Trautmann, N.: Annu. Rev. Nucl. Part. Sci. **32**, 117 (1982).
29. Münzenberg, G.: Rep. Prog. Phys. **51**, 57 (1988).
30. Trautmann, N.: Radiochim. Acta **70/71**, 237 (1995).
31. Hulet, E. K., Wild, J. F., Dougan, R. J., Lougheed, R. W., Landrum, J. H., Dougan, A. D., Baisden, P. A., Henderson, C. M., Dupzyk, R. J., Hahn, R. L., *et al.*: Phys. Rev. C **40**, 770 (1989).
32. Ichikawa, S., Tsukada, K., Asai, M., Haba, H., Sakama, M., Kojima, Y., Shibata, M., Nagame, Y., Oura, Y., Kawade, K.: Nucl. Instrum. Methods Phys. Res. B **187**, 548 (2002).
33. Asai, M. Tsukada, K., Ichikawa, S., Sakama, M., Haba, H., Nagame, Y., Nishinaka, I., Akiyama, K., Toyoshima, A., Kaneko, T., *et al.*: Eur. Phys. J. A **16**, 17 (2003).
34. Moody, K. J., Brüchle, W., Brügger, M., Gäggeler, H., Haefner, B., Schädel, M., Sümmerer, K., Tetzlaff, H., Herrmann, G., Kaffrell, N., *et al.*: Z. Phys. A **328**, 417 (1987).
35. Tetzlaff, H., Herrmann, G., Kaffrell, N., Kratz, J. V., Rogowski, J., Trautmann, N., Skalberg, M., Skarnemark, G., Alstad, J., Fowler, M. M., *et al.*: J. Less-Common Met. **122**, 441 (1986).
36. Kadkhodayan, B., Henderson, R. A., Hall, H. L., Leyba, J. D., Czerwinski, K. R., Kreek, S. A., Hannink, N. J., Gregorich, K. E., Lee, D. M., Nurmia, M. J., *et al.*: Radiochim. Acta **56**, 1 (1992).
37. Münzenberg, G.: In: *Experimental Techniques in Nuclear Physics* (Poenaru, D. N., Greiner, W., eds.) Walter de Gruyter, Berlin (1997), pp. 375–424.
38. Paul, E. S., Woods, P. J., Davinson, T., Page, R. D., Sellin, P. J., Beausang, C. W., Clark, R. M., Cunningham, R. A., Forbes, S. A., Fossan, D. B., *et al.*: Phys. Rev. C **51**, 78 (1995).
39. Leino, M., Äystö, J., Enqvist, T., Heikkinen, P., Jokinen, A., Nurmia, M., Ostrowski, A., Trzaska, W. H., Uusitalo, J., Eskola, K., *et al.*: Nucl. Instrum. Methods Phys. Res. B **99**, 653 (1995).
40. Davids, C. N., Back, B. B., Bindra, K., Henderson, D. J., Kutschera, W., Lauritsen, T., Nagame, Y., Sugathan, P., Ramayya, A. V., Walters, W. B.: Nucl. Instrum. Methods Phys. Res. B **70**, 358 (1992).
41. Reiter, P., Khoo, T. L., Lister, C. J., Seweryniak, D., Ahmad, I., Alcorta, M., Carpenter, M. P., Cizewski, J. A., Davids, C. N., Gervais, G., *et al.*: Phys. Rev. Lett. **82**, 509 (1999).
42. Herzberg, R.-D., Greenless, P. T., Butler, P. A., Jones, G. D., Venhart, M., Darby, I. G., Eeckhaudt, S., Eskola, K., Grahn, T., Gray-Jones, C., *et al.*: Nature **442**, 896 (2006).
43. Audi, G., Bersillon, O., Blachot, J., Wapstra, A. H.: Nucl. Phys. A **624**, 1 (1997).
44. Möller, P., Nix, J. R., Myers, W. D., Swiatecki, W. J.: At. Data Nucl. Data Tab. **59**, 185 (1995).
45. Möller, P., Sierk, A. J., Ichikawa, T., Iwamoto, A., Bengtsson, R., Uhrenholt, H., Åberg, S.: Phys. Rev. C **79**, 064304 (2009).
46. Lee, I. Y.: Nucl. Phys. A **520**, 641c (1990).
47. Leino, M., Kankaanpää, H., Herzberg, R.-D., Chewter, A. J., Hessberger, F. P., Coz, Y. Le, Becker, F., Butler, P. A., Cocks, J. F. C., Dorvaux, O., *et al.*: Eur. Phys. J. A **6**, 63 (1999).
48. Leino, M., Hessberger, F. P.: Annu. Rev. Nucl. Part. Sci. **54**, 175 (2004).
49. Herzberg, R.-D.: Prog. Part. Nucl. Phys. **61**, 674 (2008).
50. Sobiczewski, A., Pomorski, K.: Prog. Part. Nucl. Phys. **58**, 292 (2007).
51. Asai, M. Tsukada, K., Sakama, M., Ichikawa, S., Ishi, T., Nagame, Y., Nishinaka, I., Akiyama, K., Osa, A., Oura, Y., *et al.*: Phys. Rev. Lett. **95**, 102502 (2005).
52. Walker, P., Dracoulis, G.: Nature **399**, 35 (1999).
53. Ishii, T., Makii, H., Asai, M., Tsukada, K., Toyoshima, A., Matsuda, M., Makishima, A., Shigematsu, S., Kaneko, J., Shizuma, T.: Phys. Rev. C **78**, 054309 (2008).
54. Block, M., Ackermann, D., Blaum, K., Droese, C., Dworschak, M., Eliseev, S., Fleckenstein, T., Haettner, E., Herfurth, F., Hessberger, F. P., Hofmann, S., Ketelaer, J., *et al.*: Nature **463**, 785 (2010).
55. Bjornholm, S., Lynn, J. E.: Rev. Mod. Phys. **52**, 725 (1980).
56. Thirolf, P. G., Habs, D.: Prog. Part. Nucl. Phys. **49**, 325 (2002).
57. Krasznahorkay, A., Hunyadi, M., Harakeh, M. N., Csatlos, M., Faestermann, T., Gollwitzer, A., Graw, G., Gulyas, J., Habs, D., Hertenberger, R., *et al.*: Phys. Rev. Lett. **80**, 2073 (1998).
58. Sandulescu, A., Poenaru, D. N., Greiner, W.: Sov. J. Part. Nucl. **11**, 528 (1980).
59. Rose, H. J., Jones, G. A.: Nature (London) **307**, 245 (1984).
60. Price, P. B.: Annu. Rev. Nucl. Part. Sci. **39**, 19 (1989).
61. Poenaru, D. N., Greiner, W.: In: *Nuclear Decay Modes.* Institute of Physics Publishing, Bristol and Philadelphia (1996), Chapt. 6, p. 275.
62. Hall, H. L., Hoffman, D. C.: Annu. Rev. Nucl. Part. Sci. **42**, 147 (1992).
63. Cowan, J. J., Thielemann, F.-K., Trauran, J. W.: Phys. Rep. **208**, 267 (1991).
64. Hoffman, D. C., Hoffman, M. M.: Annu. Rev. Nucl. Sci. **24**, 151 (1974).
65. Wagemans, C.: *The Nuclear Fission Processi.* (Wagemans, C., ed.) CRC Press, Inc., Boca Raton, FL (1991), Chapt. 3, pp. 35–61.
66. Hoffman, D. C., Lane, M. R.: Radiochim. Acta **70/71**, 135 (1995).
67. Balagna, J. P., Ford, G. P., Hoffman, D. C., Knight, J. D.: Phys. Rev. Lett. **26**, 145 (1971).
68. Wild, J. F., van Aarle, J., Westmeier, W., Lougheed, R. W., Hulet, E. K., Moody, K. J., Dougan, R. J., Koop, E.-A., Glaser, R. E., Brandt, R., *et al.*: Phys. Rev. C **41**, 640 (1990).
69. Warda, M., Egido, J. L., Robledo, L. M., Pomorski, K.: Phys. Rev. C **66**, 014310 (2002).
70. Ichikawa, T., Iwamoto, A., Moller, P.: Phys. Rev. C **79**, 014305 (2009).
71. Wagemans, C., Schillebeeckx, P., Deruytter, A.: Nucl. Phys. A **502**, 287c (1989).
72. Schillebeeckx, P., Wagemans, C., Deruytter, A. J., Barthelemy, R.: Nucl. Phys. A **545**, 623 (1992).
73. Dematte, L., Wagemans, C., Barthelemy, R., D'hondt, P., Deruyter, A.: Nucl. Phys. A **617**, 331 (1997).
74. Brosa, U., Grossmann, S., Muller, A.: Phys. Rep. **197**, 167 (1990).
75. Hamilton, J. H., Ramayya, A. V., Zhu, S. J., Ter-Akopian, G. M., Oganessian, Yu. Ts., Cole, J. D., Rasmussen, J. O., Stoyer, M. A.: Prog. Part. Nucl. Phys. **35**, 635 (1995).
76. Ramayya, A. V., Hwang, J. K., Hamilton, J. H., Sandulescu, A., Florescu, A., Ter-Akopian, G. M., Daniel, A. V., Oganessian, Yu. Ts., Popeko, G. S., Greiner, W., *et al.*: Phys. Rev. Lett. **81**, 947 (1998).
77. Nagame, Y., Nishinaka, I., Tsukada, K., Oura, Y., Ichikawa, S., Ikezoe, H., Zhao, Y. L., Sueki, K., Nakahara, H., Tanikawa, M., *et al.*: Phys. Lett. B **387**, 26 (1996).
78. Möller, P., Madland, D. G., Sierk, A. J., Iwamoto, A.: Nature **409**, 785 (2001).
79. Ohtsuki, T., Nagame, Y., Nakahara, H.: In: *Heavy Elements and Related New Phenomena.* (Greiner, W., Gupta, R. J., eds.) World Scientific, Singapore (1999), Chapt. 13, pp. 507–535.
80. Zhao, Y. L., Nagame, Y., Nishinaka, I., Sueki, K., Nakahara, H.: Phys. Rev. C **62**, 014612 (2000).
81. Schmidt, K.-H., Steinhäuser, S., Böckstiegel, C., Grewe, A., Heinz, A., Junghans, A. R., Benlliure, J., Clerc, H.-G., de Jong, M., Müller, J., *et al.*: Nucl. Phys. A **665**, 221 (2000).
82. Seaborg, G. T.: Science **104**, 379 (1946)

83. Marcus, Y.: *Ion Properties*. Marcel Dekker, Inc., New York (1997).
84. Brüchle, W., Schädel, M., Scherer, U. W., Kratz, J. V., *et al.*: Inorg. Chim. Acta **146**, 267 (1988).
85. Bilewicz, A.: J. Nucl. Radiochem. Sci. **3**, 147 (2002)
86. Brewer, L.: J. Opt. Soc. Am. **61**, 1102 (1971).
87. Brüchle, W., Schädel, M., Scherer, U. W., Kratz, J. V., Gregorich, K. E., Lee, D., Nurmia, M., Chasteler, R. M., Hall, H. L., Henderson, R. A., Hoffman, D. C.: Inorg. Chim. Acta **146**, 267 (1988).
88. Toyoshima, A., Kasamatsu, Y., Tsukada, K., Asai, M., *et al.*: J. Am. Chem. Soc. **131**, 9180 (2009).
89. Antonio, M. R., Soderholm, L., Williams, C. W., Blaudeau, J. P., Bursten, B. E.: Radiochim. Acta **89**, 17 (2001).
90. Kitatsuji, Y., Kimura, T., Kihara, S.: J. Electroanal. Chem. **641**, 83 (2010).
91. Ikeda, A., Hennig, C., Rossberg, A., Funke, H., Scheinost, A. C., Bernhard, G., Yaita, T.: Inorg. Chem. **47**, 8294 (2008).
92. Takao, K., Takao, S., Scheinost, A. C., Bernhard, G., Hennig, C.: Inorg. Chem. **48**, 8803 (2009).
93. Conradson, S. D.: Inorg. Chem. **43**, 116 (2004).
94. Stumpf, S., Stumpf, T., Dardenne, K., Hennig, C., Foerstendorf, H., Klenze, R., Fanghänel, T.: Environ. Sci. Technol. **40**, 3522 (2006).
95. Denecke, M. A.: Inorg. Chem. **44**, 8418 (2005).
96. Galbis, E., Hernandez-Cobos, J., Den Auwer, C., Le Naour, C., Guillaumont, D., Simonin, E., Pappalardo, R. R., Marcos, E. S.: Angew. Chem. Int. Ed. **49**, 3811 (2010).
97. Apostolidis, C., Schimmelpfennig, B., Magnani, N., Lindqvist-Reis, P., *et al.*: Angew. Chem. Int. Ed. **49**, 6343 (2010).
98. Ghigna, P.: J. Appl. Cryst. **34**, 325 (2001).
99. Denecke, M. A.: Coord. Chem. Rev. **250**, 730 (2006).
100. http://www.gaussian.com.
101. http://www.scm.com.
102. Shamov, G. A., Schreckenbach, G.: J. Phys. Chem. A **109**, 10961 (2005).
103. Hay, P. J., Martin, R. L., Schreckenbach, G.: J. Phys. Chem. A **104**, 6259 (2000).
104. Pearson, R. G.: J. Am. Chem. Soc. **85**, 3533 (1963).
105. Horwitz, E. P., Kalina, D. G.: Solvent Extr. Ion Exch. **2**, 179 (1984).
106. Horwitz, E. P., Martin, K. A., Diamond, H., Kaplan, L.: Solvent Extr. Ion Exch. **4**, 449 (1986).
107. Muscatello, A. C., Horwitz, E. P., Kalina, D. G., Kaplan, L.: Sep. Sci. Technol. **17**, 859 (1982).
108. Sasaki, Y., Sugo, Y., Suzuki, S., Tachimori, S.: Solvent Extra. Ion Exch. **19**, 91 (2001).
109. Sasaki, Y., Tachimori, S.: Solvent Extr. Ion. Exch. **20**, 21 (2002).
110. Ansari, S. A., Mohapatra, P. K., Manchanda, V. K.: Ind. Eng. Chem. Res. **48**, 8605 (2009).
111. Musikas, C.: *Actinide-Lanthanide Separation, International Symposium Proceedings*. (Choppin, G. R., Navratil, J. D., Schulz, W. W., eds.) World Scientific, Singapore (1985), pp. 19–30.
112. Zhu, Y.: Radiochim. Acta **68**, 95 (1995).
113. Zhu, Y., Chen, J., Jiao, R.: Solvent Extr. Ion. Ech. **14**, 61 (1996).
114. Chen, J., Zhu, Y., Jiao, R.: Sep. Sci. Technol. **31**, 2723 (1996).
115. Klaehn, J. R., Peterman, D. R., Harrup, M. K., Tillotson, R. D., Luther, T. A., Law, J. D., Daniels, L. M.: Inorg. Chim. Acta **361**, 2522 (2008).
116. Cao, X., Heidelberg, D., Ciupka, J., Dolg, M.: Inorg. Chem. **49**, 10307 (2010).
117. Kolarik, Z., Müllich, U., Gassner, F.: Solv. Extr. Ion Exch. **17**, 1155 (1999).
118. Kolarik, Z.: Chem. Rev. **108**, 4208 (2008).
119. Madic, C., Hudson, M. J., Liljenzin, J. O., Glatz, J. P., Nannicini, R., Facchini, A., Kolarik, Z., Odoj, R.: New partitioning techniques for minor actinides. EUR 19149 EN (2000).
120. Guillaumont, D.: J. Mol. Struct. Theochem. **771**, 105 (2006).
121. Hill, C., Guillaneaux, D., Berthon, L., Madic, C.: J. Nucl. Sci. Technol. Suppl. **3**, 289 (2002).
122. Drew, M. G. B., Foreman, M. R. S. J., Hill, C., Hudson, M. J., Madic., C.: Inorg. Chem. Commun. **8**, 239 (2005).
123. Haire, R. G.: J. Alloys Compd. **444/445**, 63 (2007).
124. Stephans, D. R., Stromberg, H. D., Lilley, E. M.: J. Phys. Chem. Solids **29**, 81 (1968).
125. Skriver, H. L., Andersen, O. K., Johansson, B.: Phys. Rev. Lett. **44**, 1230 (1980).
126. Benedict, U.: *Handbook on the Physics and Chemistry of the Actinides*. (Freeman, A. J., Lander, G. H., eds.) Elsevier Science Publishers, Amsterdam (1987), Chap. 3, pp. 227–269.
127. Benedict, U., Holzapfel, W. B.: *Handbook on the Physics and Chemistry of Rare Earthes, Vol. 17, Lanthanides/Actinides: Physics-1*. (Gschneidnew, K. A., Eyring, L., Lander, G. H., Choppin, G. R., eds.) Elsevier Science Publishers, Amsterdam (1993), Chapt. 113, pp. 245–300.
128. Heathman, S., Haire, R. G., Le Bihan, T., Lindbaun, A., Litfin, K., Meresse, Y., Libotte, H.: Phys. Rev. Lett. **85**, 2961 (2000).
129. Lindbaum, A., Heathman, S., Litfin, K., Merese, Y., Haire, R. G.: Phys. Rev. B **63**, 214101 (2001).
130. Söderlind, P., Landa, A.: Phys. Rev. B **72**, 024109 (2005).
131. Moore, K. T., van der Laan, G., Haire, R. G., Wall, M. A., Schwartz, A. J., Söderlind, P.: Phys. Rev. Lett. **98**, 236402 (2007).
132. Marianetti, C. A., Haule, K., Kotliar, G., Fluss, M. J.: Phys. Rev. Lett. **101**, 056403 (2008).
133. Petit, L., Svane, A., Szotek, Z., Temmerman, W. M., Stocks, G. M.: Phys. Rev. B **81**, 045108 (2010).
134. Wang, B. T., Shi, H., Li, W., Zhang, P.: Phys. Rev. B **81**, 045119 (2010).
135. Tokunaga, Y., Nishi, T., Kambe, S., Nakada, M., Itoh, A., Homma, Y., Sakai, H., Chudo, H.: J. Phys. Soc. Jpn. **79**, 053705 (2010).
136. Walstedt, R. E., Kambe, S., Tokunaga, Y., Sakai, H.: J. Phys. Soc. Jpn. **76**, 072001 (2007).
137. Hardy, G. F., Hulm, J. K.: Phys. Rev. **93**, 1004 (1954).
138. Berlincourt, T. G.: Phys. Rev. **114**, 969 (1959).
139. Sarrao, J. L., Morales, L. A., Thompson, J. D., Scott, B. L., Stewart, G. R., Wastin, F., Rebizant, J., Boulet, P., Colineau, E., Lander, G. H.: Nature **420**, 297 (2002).
140. Curro, N. J., Caldwell, T., Bauer, E. D., Morales, L. A., Graf, M. J., Bang, Y., Balatsky, A. V., Thompson, J. D., Sarrao, J. L.: Nature **434**, 622 (2005).
141. Aoki, D., Haga, Y., Matsuda, T. D., Tateiwa, N., Ikeda, S. *et al.*: J. Phys. Soc. Jpn. **76**, 063701 (2007).
142. Yamagami, H., Aoki, D., Haga, Y., Onuki, Y.: J. Phys. Soc. Jpn. **76**, 083708 (2007).
143. Monthoux, P., Pines, D., Lonzarich, G. G.: Nature **450**, 1177 (2007).
144. Dai, X.: Science **300**, 953 (2003).
145. Shim, J. H.: Nature **446**, 513 (2007).
146. Olander, D.: J. Nucl. Mater. **389**, 1 (2009).
147. IAEA Nuclear Energy Series No. NF-T-4.6, IAEA Vienna (2009).
148. Kassner, M. E., Peterson, D. E. (eds.): *PhaseDiagrams of Binary Actinide Alloys*. Monograph Series on Alloy Phase Diagrams **11**, The Materials Information Society, USA (1995).
149. Havela, L., Gouder, T., Wastin, F., Rebizant, J.: Phys. Rev. B **65**, 235118 (2002).
150. Espinosa, F. J., Villella, P. Lashley, J. C., Conradson, S. D., Cox, L. E., Martinez, B., Morales, L., Terry, J., Pereyra, R. A.: Phys. Rev. B **63**, 174111 (2001).
151. Allen, P. G., Henderson, A. L., Sylwester, E. R., Turchi, P. E. A., Shen, T. H., Gallegos, G. F., Booth, C. H.: Phys. Rev. B **65**, 214107 (2002).
152. Söderlind, P., Land, A., Sadigh, B.: Phys. Rev. B. **66**, 205109 (2002).
153. Savrasov, S. Y., Kotliar, G., Abrahams, E.: Nature **410**, 793 (2001).
154. Georges, A., Kotliar, G., Krauth, W., Rozenberg, J. J.: Rev. Mod. Phys. **68**, 13 (1996).
155. Nishi, T., Nakada, M., Suzuki, C., Shibata, H., Itoh, A., Akabori, M., Hirata, M.: J. Nucl. Mater. **401**, 138–142 (2010).
156. Martin, P. M., Belin, R. C., Valenza, P. J., Scheinost, A. C.: J. Nucl. Mater. **385**, 126 (2009).